Author Manuscript
Author Manuscript
Author Manuscript
Author Manuscript

HHS Public Access
Author manuscript
Nat Cancer. Author manuscript; available in PMC 2021 April 22.

Published in final edited form as:
Nat Cancer. 2021 April ; 2(4): 444–456. doi:10.1038/s43018-021-00185-w.

EZH2 inhibition activates a dsRNA–STING–interferon stress axis that potentiates response to PD-1 checkpoint blockade in prostate cancer

Katherine L. Morel[#1], **Anjali V. Sheahan**[#1], **Deborah L. Burkhart**[1], **Sylvan C. Baca**[2], **Nadia Boufaied**[3], **Yin Liu**[4], **Xintao Qiu**[2], **Israel Cañadas**[5], **Kevin Roehle**[6], **Max Heckler**[6], **Carla Calagua**[7], **Huihui Ye**[8], **Constantia Pantelidou**[2], **Phillip Galbo**[9], **Sukanya Panja**[10], **Antonina Mitrofanova**[10,11], **Scott Wilkinson**[12], **Nichelle C. Whitlock**[12], **Shana Y. Trostel**[12], **Anis A. Hamid**[2], **Adam S. Kibel**[13], **David A. Barbie**[2], **Atish D. Choudhury**[2], **Mark M. Pomerantz**[2], **Christopher J. Sweeney**[2], **Henry W. Long**[2], **David J. Einstein**[14], **Geoffrey I. Shapiro**[2], **Stephanie K. Dougan**[6], **Adam G. Sowalsky**[12], **Housheng Hansen He**[4], **Matthew L. Freedman**[2], **Steven P. Balk**[14], **Massimo Loda**[15], **David P. Labbé**[3,16], **Brian M. Olson**[17], **Leigh Ellis**[1,18,19,20,21,✉]

[1]Department of Oncologic Pathology, Dana-Farber Cancer Institute, Boston, MA, USA.

[2]Department of Medical Oncology, Dana-Farber Cancer Institute, Boston, MA, USA.

[3]Cancer Research Program, Research Institute of the McGill University Health Centre, Montréal, Canada.

[4]Department of Medical Biophysics, University of Toronto and Princess Margaret Cancer Center University Health Network, Toronto, Canada.

[5]Blood Cell Development and Function Program, Fox Chase Cancer Center, Philadelphia, PA, USA.

[6]Department of Cancer Immunology and Virology, Dana-Farber Cancer Institute, Boston, MA, USA.

[7]Department of Medicine, Hematology-Oncology Division, Beth Israel Deaconess Medical Center, Harvard Medical School, Boston, MA, USA.

✉**Correspondence and requests for materials** should be addressed to L.E., Leigh.Ellis@cshs.org.

Author contributions
K.L.M., A.V.S., D.L.B. and B.M.O. performed research, analyzed data and wrote the manuscript. S.C.B., D.P.L., C.C., H.Y., P.G., S.P., A.M., A.A.H., C.J.S. and M.L. performed research. K.R., M.H., S.K.D., A.D.C., N.B., Y.L., H.H.H., A.G.S., M.M.P., M.L.F., S.W., N.C.W., S.Y.T., A.G.S., C.P., G.I.S., X.Q. and H.W.L. provided vital reagents. A.D.C., D.P.L., H.Y., M.L.F., S.C.B., C.J.S., D.J.E., S.K.D., A.G.S., S.P.B. and B.M.O. assisted with editing the final manuscript. L.E. designed experiments, analyzed data and wrote the manuscript.

Competing interests
The authors declare no competing interests.

Extended data is available for this paper at https://doi.org/10.1038/s43018-021-00185-w.

Supplementary information The online version contains supplementary material available at https://doi.org/10.1038/s43018-021-00185-w.

Peer review information *Nature Cancer* thanks Mark A. Rubin, Weiping Zou and the other, anonymous, reviewer(s) for their contribution to the peer review of this work. Peer review reports are available.

Reprints and permissions information is available at www.nature.com/reprints.

Author Manuscript Author Manuscript Author Manuscript Author Manuscript

[8]Department of Pathology, University of California at Los Angeles, Los Angeles, CA, USA.

[9]Department of Cell Biology, Albert Einstein College of Medicine, Bronx, NY, USA.

[10]Department of Health Informatics, Rutgers School of Health Professionals, Newark, NJ, USA.

[11]Rutgers Cancer Institute of New Jersey, Rutgers, The State University of New Jersey, New Brunswick, NJ, USA.

[12]Laboratory of Genitourinary Cancer Pathogenesis, Center for Cancer Research, National Cancer Institute, National Institutes of Health, Bethesda, MD, USA.

[13]Department of Urology, Brigham and Women's Hospital, Harvard Medical School, Boston, MA, USA.

[14]Hematology and Oncology Division, Department of Medicine, Beth Israel Deaconess Medical Center and Harvard Medical School, Boston, MA, USA.

[15]Department of Pathology and Laboratory Medicine, Weill Cornell Medicine, New York, NY, USA.

[16]Division of Urology, Department of Surgery, McGill University, Montréal, Canada.

[17]Departments of Hematology and Medical Oncology and Urology, Emory University School of Medicine, Atlanta, GA, USA.

[18]Department of Pathology, Brigham and Women's Hospital, Harvard Medical School, Boston, MA, USA.

[19]Cancer Program, The Broad Institute of MIT and Harvard, Cambridge, MA, USA.

[20]Division of Medical Oncology, Department of Medicine, Cedars-Sinai Medical Center, Los Angeles, CA, USA.

[21]Cedars-Sinai Samuel Oschin Comprehensive Cancer Institute, Los Angeles, CA, USA.

[#] These authors contributed equally to this work.

Abstract

Prostate cancers are considered to be immunologically 'cold' tumors given the very few patients who respond to checkpoint inhibitor (CPI) therapy. Recently, enrichment of interferon-stimulated genes (ISGs) predicted a favorable response to CPI across various disease sites. The enhancer of zeste homolog-2 (EZH2) is overexpressed in prostate cancer and known to negatively regulate ISGs. In the present study, we demonstrate that EZH2 inhibition in prostate cancer models activates a double-stranded RNA–STING–ISG stress response upregulating genes involved in antigen presentation, Th1 chemokine signaling and interferon response, including programmed cell death protein 1 (PD-L1) that is dependent on STING activation. EZH2 inhibition substantially increased intratumoral trafficking of activated $CD8^+$ T cells and increased M1 tumor-associated macrophages, overall reversing resistance to PD-1 CPI. Our study identifies EZH2 as a potent inhibitor of antitumor immunity and responsiveness to CPI. These data suggest EZH2 inhibition as a therapeutic direction to enhance prostate cancer response to PD-1 CPI.

Prostate cancer (PCa) is currently the most commonly diagnosed noncutaneous malignancy and the second most common cause of cancer death among men in the United States[1].

Author Manuscript Author Manuscript Author Manuscript Author Manuscript

Unfortunately, metastatic castration-resistant PCa (mCRPC) still remains incurable, despite recent advances in therapy options for these patients. Although CPI can generate dramatic responses in about 15–20% of patients with a number of cancer types, including melanoma, kidney and bladder cancer, this occurs in approximately 5% of PCa patients. Resistance toward CPI in PCa patients is thought to be related to low tumor immunogenicity and an immunosuppressive tumor microenvironment.

EZH2 is the methyltransferase catalytic subunit of the polycomb repressive complex 2 (PRC2) that trimethylates Lys27 of histone H3 (H3K27me3) to promote transcriptional repression[2]. Increased expression and activity of EZH2 are important contributors to PCa initiation and progression[3,4]. EZH2 can negatively regulate ISGs, including Th1-type chemokines, immune checkpoint molecules like PD-L1 and major histocompatibility complex (MHC) expression in multiple tumor cell types[5,6]. More recently, it had been shown that silencing of MHC-I antigen-processing genes was mediated by coordinated transcriptional silencing by PRC2 (ref.[7]). Likewise, diffuse large B-cell lymphomas harboring EZH2-activating mutations exhibit low expression of MHC-I and MHC-II molecules[6]. Together, tumors with increased function of EZH2 often display immunosuppressive tumor microenvironments and immunotherapy resistance.

Dysfunction of epigenetic regulation within a cancer cell, including effects mediated by EZH2, DNA methytransferases, histone deacetylases, BET bromodomains and lysine-specific demethylase 1 have proven to be critical mediators of acquired tumor immune escape. Subsequent inhibition of these epigenetic mechanisms results in increased tumor immunity and successful combination with CPI in preclinical cancer models[5,8–15]. Importantly, recent data from a phase Ib/II clinical trial, ENCORE-601 (NCT02437136), illustrated the power of epigenetic therapy to restore sensitivity in a subset of melanoma patients who had progressed on an inhibitor of PD-1 (ref.[16]).

Targeting epigenetic mechanisms mediated by EZH2 have not been tested for their ability to induce response to CPI in PCa. In the present study, we demonstrate that chemical and genetic inhibition of EZH2's catalytic function derepresses endogenous dsRNA, leading to a notable induction of ISGs in PCa tumor cells. Activation of this dsRNA–ISG tumor cell response by EZH2 inhibition is dependent on activation of the stimulator of interferon (IFN) genes (STING) and leads to reversal of resistance to anti-PD-1 therapy in B6-MYCCaP PCa tumors in vivo. Overall, these data provide important evidence for targeting chromatin and epigenetic regulators such as EZH2 to overcome immunotherapy resistance in PCa.

Results

Using three-dimensional (3D) tumor organoids derived from a genetically engineered mouse model of PCa (GEMM) that expresses oncogenic *cMYC*[17], *Ezh2* floxed alleles[18] and an inducible *Cre* recombinase driven by the prostate-specific antigen (PSA) promoter[19] (EMC mouse) we demonstrated that genetic or chemical inhibition of EZH2 catalytic activity resulted in diminished organoid growth (Fig. 1a,b), accompanied by a significant decrease in DNA synthesis and H3K27me3 (Fig. 1a,b). RNA-sequencing (RNA-seq) and gene set enrichment analysis (GSEA) revealed enrichment of type I (IFN-α) and II (IFN-γ) gene

Author Manuscript Author Manuscript Author Manuscript Author Manuscript

signatures (Fig. 1c and Extended Data Fig. 1). Interrogation of leading-edge genes related to IFN signaling from mouse PCa organoids revealed increases in expression of Th1 chemokines (*Cxcl9*, *Cxcl10* and *Cxcl11*), antigen-presentation genes (*B2m* and *Tap1*) and IFN-γ-regulated genes (*Stat1* and *CD274*/*Pd-l1*). The enrichment of IFN-response genes was further corroborated when master regulator (MR) analysis using MARINa was applied to both RNA-seq datasets from 1C to identify transcription factors (TFs) driving this pattern of gene expression. Overlap of both MR lists (top 200 ranked by NES, normalized enrichment score) showed that a set of 36 TFs was common in both conditions. These included important machinery for control of ISGs including *Stat1*, *Icam1*, *Ifi16*, *Sp100*, *Trim22*, *Trim29*, *Irf1*, *Irf8* and *Irf9* (Fig. 1d and Supplementary Table 1). Specifically, Stat1 and Irf proteins are shown to form transcriptional machinery that regulates ISG expression[20].

To determine whether loss of EZH2 catalytic activity was associated with enrichment of ISGs in human PCa, a 29-gene EZH2 repression signature was derived using differentially expressed (DE) genes after chemical inhibition of EZH2 from Fig. 1c (Supplementary Table 2) applied to independent human PCa RNA-seq datasets (Supplementary Table 3). Previously, an independent EZH2 repression signature was reported[21] and, although both signatures were mutually exclusive, they were significantly correlated with each other (Extended Data Fig. 1). Of importance, EZH2 activity was not altered because of changes in *EZH2* gene expression (Extended Data Fig. 1). On quartile distribution of patients, differential gene expression between quartile 4 (lowest EZH2 activity) and quartile 1 (highest EZH2 activity) validated our in vitro murine results by indicating that patients with the lowest EZH2 activity were enriched for type I/II IFN-response genes (Fig. 1e and Extended Data Fig. 2). In line with our in vitro data, low EZH2 activity in PCa patients was also associated with increased expression of Th1 chemokines (*CXCL10* and *CXCL11*), antigen-presentation genes (*B2M* and *HLA-A*) and IFN-γ-regulated genes (*STAT1* and *IRF9*) (Extended Data Fig. 2).

Recently, epigenetic targeted therapies were shown to induce ISGs by derepression of dsRNA[8,10,11]. This mechanism, termed ‘viral mimicry’, involves the re-expression of dormant transposable elements after treatment with epigenetic therapies[8,10,11]. This instructs the cancer cell to adapt and respond as if infected by an exogenous virus and mount an innate immune defense via induction of dsRNA sensor machinery and ISGs[22]. Treatment with EZH2 inhibitors significantly induced total intracellular levels of dsRNA in murine and human 3D PCa organoids (Fig. 2a), and in murine PCa tissue in vivo (Fig. 2b). Using immunofluorescence, human prostatectomy samples with >5% tumor PD-L1 expression (PD-L1 high) exhibited low H3K27me3 levels and increased dsRNA levels. Adversely, patient samples with <5% tumor PD-L1 positivity (PD-L1 low) demonstrated high H3K27me3 expression and low dsRNA expression (Fig. 2c,d and Supplementary Table 4). In accordance with these data we also found increased expression of innate immune receptors including STING and toll-like receptor 3 (TLR3) (Fig. 4a and Extended Data Fig. 2), and dsRNA sensors RIG-I and MDA5 (Extended Data Fig. 2) occurred in patient samples with low EZH2 activity. Also enriched in patients with low EZH2 activity were a novel subclass of endogenous retroviral sequences (ERVs) contained in genes co-regulated by STAT1 and EZH2 called stimulated prime antisense retroviral coding sequences (SPARCS).

Author Manuscript Author Manuscript Author Manuscript Author Manuscript

SPARCS genes housing ERVs were demonstrated to induce an innate immune response on expression (Extended Data Fig. 2)[23]. We next overlaid both mouse and human IFN-α/γ DE genes from Fig. 1 and identified an overall 97-gene IFN gene signature (Extended Data Fig. 3). It is interesting that, although SPARC gene expression is shown to be induced by IFN treatment, only 1 SPARC gene (*IFI44L*) appeared in our 97-gene IFN gene signature. It was also observed that our gene set did include enrichment of *IFI44*, *IFI27* and *OASL*, which are type I IFN-stimulated 'viral mimicry' genes shown to be upregulated by DNA methyltransferase inhibition[24,25]. Moreover, there was an enrichment of biological and molecular Gene Ontology terms, including innate immune response, dsRNA binding and Tap binding (Extended Data Fig. 3).

To further understand mechanisms underlying the observed increased expression of ISGs by EZH2 inhibition, we utilized published human PCa patient and cell-line chromatin immunoprecipitation (ChIP)-seq datasets[26–28]. In human patient samples, our 97 ISGs did not display overall enrichment for H3K27me3, indicating that no direct repression of these genes is regulated by EZH2 catalytic activity (Fig. 3a). Instead, we found that these genes contain enrichment of H3K27ac and open chromatin regions (Fig. 3a and Extended Data Fig. 3). Likewise, we observed, in LNCaP cell lines treated with genetic or chemical inhibition of EZH2, enrichment of IFN-α/γ gene sets (Extended Data Fig. 3). Furthermore, EZH2 inhibition in LNCaP cells exhibited a dramatic increase in H3K27ac at these ISGs (Fig. 3b). As expression of these ISGs was dramatically increased after treatment with epigenetic therapies, it suggests that these genes are primed for rapid activation. As we had already observed a significant induction of tumor cell dsRNA levels after EZH2 inhibition (Fig. 2), we further analyzed H3K27me3 and H3K27ac locations in LNCaP cells. We observed a total of 302 genes that contained ERVs within their 3′-UTR (Supplementary Table 5) which, on EZH2 inhibition, resulted in direct loss of H3K27me3 and concurrent gain of H3K27ac (Fig. 3c,d). These data indicate that direct derepression of ERVs catalyzes the increased expression of ISGs after EZH2 inhibition.

As stated, multiple regulators that drive viral defense mechanisms, including STING, were upregulated in PCa patient tumors with low EZH2 activity (Fig. 4a and Extended Data Fig. 2). To validate a molecular link between endogenous tumor cell dsRNA and ISG upregulation by EZH2 inhibition, we used both chemical and genetic methods to attenuate STING function in two independent murine PCa cell lines. These cell lines either overexpressed *MYC* or harbored loss of *Pten*. STING was expressed in both cell lines (Fig. 4b) and loss of STING activity did not affect the induction of dsRNA by EZH2 inhibition, but did significantly suppress the ability of EZH2 inhibition to induce MHC-I and PD-L1 expression (Fig. 4c and Extended Data Fig. 4). These results demonstrate the importance of STING for upregulation of genes critical for increasing anti-cancer immunogenicity in response to EZH2 inhibition.

We next proposed that EZH2 inhibition would sensitize PCa tumors in vivo to PD-1 CPI. Support of this proposition was indicated by human PCa samples with low EZH2 activity being significantly enriched for two gene signatures demonstrated to predict response to CPI. These are a MImm score[29] and a T-cell-inflamed gene signature[30] (Extended Data Fig. 5). Using a B6-Hi*MYC* PCa transgenic tissue transplant model[17], EZH2 inhibition (EPZ) or

Author Manuscript Author Manuscript Author Manuscript Author Manuscript

PD-1 CPI did not display antitumor activity individually; however, combination treatment produced a significant therapeutic effect without extensive toxicity (Fig. 4b and Extended Data Fig. 5). EZH2 inhibition in vivo was also associated with loss of tumor H3K27me3 levels and increased tumor expression of PD-L1 (Extended Data Fig. 5 and Fig.5b). Also noted was a reduction of PD-1 in tumor-infiltrating $CD8^+$ but not $CD4^+$ T cells (Extended Data Fig. 7). We further validated the ability of EZH2 inhibition to increase gene and protein expression of PD-L1 in murine and human PCa models (Fig. 5c and Extended Data Fig. 5). In addition, correlation analysis of patient PCa samples indicated that the patients with the lowest EZH2 activity had substantial enrichment of PD-L1 gene expression (Extended Data Fig. 5). As the significant induction of PD-L1 expression was dependent on STING in PCa models after treatment with EZH2 inhibitors, we sought to determine whether increased PD-L1 was functionally relevant. For this, we used an in vitro cytotoxicity assay. Using our murine PCa cell lines on a B6 background with either wild-type PD-L1 or knockout (KO) PD-L1 (Extended Data Fig. 6), we pretreated tumor cells with dimethylsulfoxide (DMSO) or an EZH2 inhibitor before co-incubation with murine splenocytes on an FVB background and evaluated immune cytotoxicity (Fig. 5d). Our results clearly demonstrated that inhibition of EZH2 activity resulted in a significant loss of immune-mediated cytotoxicity, which was dependent on tumor cell upregulation of PD-L1. Strikingly, immune-mediated cytotoxicity was restored in EZH2 inhibitor-treated cell lines by the addition of a PD-1 antibody, and this combination effect was also dependent on tumor PD-L1 upregulation (Fig. 5d).

Further assessment of the tumor microenvironment revealed that EZH2 inhibition and combination groups showed increased accumulation of $CD4^+$ and $CD8^+$ T cells (Fig. 6a). No change to intratumoral frequency of regulatory T cells (T_{reg} cells) was observed (Extended Data Fig. 7). Although both $CD4^+$ and $CD8^+$ T-cell trafficking was increased, only $CD8^+$ T cells were significantly activated in PD-1 CPI and combination groups (Fig. 6b). With this observed increase in T-cell trafficking, we further interrogated whether EZH2 inhibition could increase Th1 chemokine expression in tumor cells. We treated both B6-MYCCaP and Pten KO murine PCa cell lines with the EZH2 inhibitors DZNep and EPZ. Overall, inhibition of EZH2 activity resulted in a drastic upregulation of Th1 chemokines interleukin (IL)-2, IL-12 p40p70, IL-12 p70 and tumor necrosis factor α (TNF-α). There was no observed upregulation of IFN-γ in cell lines by either EZH2 inhibitor (Fig. 6c and Extended Data Fig. 6). Analysis of gene expression data from patient tumor samples further validated that low EZH2 activity was most associated with increased expression of Th1 cytokines. Th2 and Th17 cytokines[31] were less rep-resented in tumors with low EZH2 activity (Extended Data Fig. 6). Additional evaluation of the microenvironment also showed no significant alterations in the frequency of myeloid or granulocytic myeloid-derived suppressor cells (MDSCs; Extended Data Fig. 7); however, significant increases of intratumoral M1 tumor-associated macrophages (TAMs), with concurrent loss of M2 TAMs, were observed in EPZ, PD-1 CPI and combination-treated groups (Fig. 7). Overall, combination treatment provided the most significant increase in the M1:M2 TAM ratio. In concordance with our data, it was shown that inhibition of PRC1 in double-negative PCa models resulted in increased T-cell tumor infiltration and decreased immunosuppressive cells, and provided superior therapeutic benefit when combined with CPI[32], implicating polycomb complexes as important meditators for immunotherapy response in PCa.

Author Manuscript Author Manuscript Author Manuscript Author Manuscript

Discussion

Identifying mechanisms driving resistance toward CPIs in PCa patients remain a critical requirement. Although progress has been made describing molecular events that increase response, including patients with DNA-damage repair pathway defects[33,34], biallelic loss of CDK12 (ref.[35]), recycling of PD-L1 in patients lacking a common mutation in speckle-type POZ protein (SPOP)[36] and inhibition of IL-23 (ref.[37]), most patients currently treated with CPI remain unresponsive.

Epigenetic regulation of immunogenicity has become one major focus to delineate mechanisms utilized by tumors to evade immune system eradication and resistance to currently available immunotherapies, specifically CPIs. It is becoming more evident that the primary mechanism mediated by epigenetic regulators is the repression of repeat element sequences (dsRNA) and immune response genes. Our work demonstrates that, in PCa models and patient samples, loss of EZH2 catalytic function results in the derepression of dsRNA and genes involved with IFN response, antigen presentation and T-cell attraction. In addition, we demonstrate that detection of increased dsRNA levels and subsequent gene response is dependent on intratumoral PD-L1 and STING activation and function. It will be important to further delineate whether activation of STING is due to dsRNA detection via crosstalk with RIG-I or whether dsRNA is being converted by reverse transcription to dsDNA. Reverse transcription of dsRNA to dsDNA may result in presentation of exclusive tumor cell antigens. This discovery could result in the production of personalized vaccine approaches that may be placed in combination strategies with epigenetic therapies such as EZH2 inhibitors.

Importantly, our work and that of others demonstrate that epigenetic targeted therapies reprogram the tumor microenvironment by a positive effect on T-cell populations. Epigenetic mechanisms, including those mediated by EZH2, have been shown to inhibit overall T-cell differentiation and tumor infiltration[38]. Specific to EZH2, it has been demonstrated as an important regulator of differentiation in $CD4^+$ T cells and T_{reg} cells[39,40]. In T_{reg} cells, loss of EZH2 resulted in degradation of FOXP3, allowing T_{reg} cells to be reprogrammed to a T-helper cell phenotype[41]. Our in vivo data did not show a change to total T_{reg} intratumoral numbers, but do induce a significant increase in $CD4^+$ and $CD8^+$ T cells within the tumor microenvironment. In addition, we induced downregulation of PD-1 expression in $CD8^+$ T cells by EZH2 inhibition, suggesting a reversal of exhaustion that allows for their ability to be reactivated through a combination with anti-PD-1 therapy. Most exciting, in human studies, the inhibition of EZH2 in $CD8^+$ T cells by CPI-1205 has resulted in increasing cytotoxic activity[41].

MDSCs have also been demonstrated to be an important component of an immunosuppressive tumor microenvironment. Specific to PCa, a subset of patients with CRPC were shown to have their AR signaling activated by MDSC-secreted IL-23 (ref.[37]). Our data indicated that EZH2 inhibitor monotherapy or combination did not dramatically alter MDSC tumor infiltrate populations. Instead, we identified a significant effect by EZH2 inhibition and combination treatments on TAM tumor infiltrate composition. TAMs can be polarized to be tumor inhibiting (M1 TAMs) or tumor promoting (M2 TAMs). M2 TAMs

Author Manuscript Author Manuscript Author Manuscript Author Manuscript

have also been shown to be a major component of the immunosuppressive PCa microenvironment[42]. B6-Hi*MYC* tumors displayed a considerable increase in M2 TAMs, which were significantly decreased after treatment, while, conversely, M1 TAMs were dramatically increased, overall supporting reprogramming toward an antitumor microenvironment.

Our study provides vital insight into how epigenetic mechanisms mediated by EZH2 drive resistance toward CPI in PCa. Collectively, EZH2 inhibition in tumor cells induces dsRNA intracellular stress, resulting in an increased STING–ISG response, reprogramming of TAM infiltration, promotion of $CD8^+$ T-cell activation and sensitivity to PD-1 blockade in vivo. These findings provide a substantial insight into PCa tumor immunity and propose the potential for patient stratification by EZH2 activity, generating the rationale to develop combinatorial use of EZH2 inhibitors with PD-1 CPI as a strategy to increase PCa response to checkpoint immunotherapy.

Methods

Further information on the research design is available in the Nature Research Reporting Summary linked to this article. Patient prostatectomy samples used for organoid generation were collected under Dana-Farber Cancer Institute protocol nos. 01–045 and 09–171 with patient consent. All remaining patient samples/data used in the present study had been collected with patient consent obtained by the respective studies.

Experimental models.

The Institute of Animal Care and Use Committee at the Dana-Farber Cancer Institute approved all mouse procedures. C57BL/6N and FVB mice were obtained from Charles River Labs (strains 027 and 207, respectively). $Pten^{f/f}$;Pb-Cre, Pb-HiMYC, $Ezh2^{fl/fl}$ and PSA-Cre(ERT2) strains have been described previously[17,19,43–46]. All models were validated by genotyping PCR analysis before use in subsequent studies using genomic DNA extracted from mouse ears or tails. Genotyping primers used are detailed in Supplementary Table 7. The $Ezh2^{fl/fl}$; Pb-HiMYC;PSA-Cre(ERT2)^{pos} mice (EMC mouse strain) generated in the present study were of a mixed background consisting of FVBN and C57Bl/6.

Organoid models were generated using previously described methods and maintained as previously published[47]. Clinical samples were provided under institutional review board (IRB) approval (protocol no. 17–571; L.E.). Human organoids were generated from two independent patient samples: (1) prostatectomy and (2) pleural effusion sample provided by A. Kibel and A. Choudhury, respectively (IRB protocol no.: 01–045; Gelb Center DFCI/HCC). Murine EMC organoids were generated from the dorsolateral prostates of 8-week-old GEMMs, whereas the $Pten^{-/-}$ 3D organoids were generated from end-stage prostate tumors at age 61 weeks. Mouse organoids were validated by genotyping and recombination PCRs. The primers are detailed in Supplementary Table 7.

$Pten^{-/-}$ and B6MYC-CaP murine cell lines have been previously described[17,48]. LNCaP cells were obtained from American Type Culture Collection. PD-L1 KO models and controls were generated using pSPCas9(BB)-2A-Puro (PX459) v.2.0, which was a gift from F. Zhang

Author Manuscript Author Manuscript Author Manuscript Author Manuscript

(Addgene plasmid no. 62988: http://n2t.net/addgene:62988)[49]. PD-L1 KO and control cells were generated by transfecting with the PX459;sgPD-L1 or empty PX459 vector using Lipofectamine 2000 DNA Transfection Reagent (Thermo Fisher Scientific, catalog no. 11668) following the manufacturer's instructions. Cells were selected with puromycin. PD-L1 KO was validated by quantitative PRCR with reverse transcription PCR (RT–qPCR) after stimulation with 100 U ml^{-1} of IFN-γ. STING KO and control cell lines were generated as described in Pantelidou et al.[50] and used as a pooled population for all experiments. STING KO was validated by western blotting.

Mouse cytokine arrays.

Mouse cell lines were treated with DZNep (5 μM), EPZ (5 μM), IFN-γ (100 U ml^{-1}) or DMSO control for 4 d, with medium and drugs changed on day 2. Th1-related cytokine changes were analyzed by mouse cytokine antibody array (Abcam, ab133993) according to the manufacturer's instructions.

Therapy experiments.

In vitro assays.—For all in vitro therapy experiments, cells were seeded at the following concentrations: two-dimensional (2D) cell lines were seeded at a concentration of 25,000 cells per well of a 24-well plate; organoids were seeded at a concentration of 20,000 cells per 40 μl of Matrigel disk. In both cases, each well was treated with either 1 μM or 5 μM DZNep or EPZ6438, DMSO or 100 U ml^{-1} of IFN-γ control.

In vitro cytotoxicity assay.—The spleens from FVB mice were mashed through a sterile 40-μm cell strainer (Corning) that had been pre-wetted with sterile phosphate-buffered saline (PBS; Gibco). Red blood cells were lysed using a commercial ACK Lysing Buffer (Gibco). Splenocytes were stored at 2×10^7 cells ml^{-1}. Cultures were treated with 5 μM DZNep or EPZ6438, or DMSO control for 4 d. After EZH2 inhibitor treatment, tumor cells were washed with PBS, digested to a single-cell suspension with TrypLE (Gibco) and washed with Dulbecco's modified Eagle's medium (DMEM) with 10% fetal bovine serum (FBS). After washing by centrifugation, cells were resuspended in DMEM + 10% FBS, and re-plated into nonadherent, 96-well, round-bottomed plates. Cells were allowed to incubate with 10 μg ml^{-1} of anti-mouse PD-1 antibody or immunoglobulin (Ig)G control for 30 min at room temperature (Supplementary Table 6). After incubation, splenocytes derived from FVB mice were added at a tumor cell:splenocyte ratio of 1:10. Cells were co-cultured with splenocytes for 8 h, after which the plates were spun down and 50 μl of supernatant was extracted for assessment of cytotoxicity. Cytotoxicity was measured using the CytoTox 96 Non-Radioactive Cytotoxicity Assay (Promega) according to the manufacture's instructions. Cytotoxicity was measured using a SpectraMax plate reader (Molecular Devices).

In vivo therapy experiment.—Pb-HiMyc-derived tumor tissue[17] was sectioned into 2-mm^2 tumor chunks and subcutaneously implanted into syngeneic C57BL/6N mice (Charles River Labs). Then, 4 d after the implant, mice were treated with either 250 mg kg^{-1} of EPZ0011989 (Epizyme) or 0.5% carboxymethylcellulose by oral gavage twice daily, 200 μg of anti-PD-1 (29F.1A12) or IgG control (2A3) by intraperitoneal injection every 3 d, started on day 5 after initiation of EZH2 inhibition therapy, or a combination (Supplementary Table

Author Manuscript Author Manuscript Author Manuscript Author Manuscript

6). Tumors and mouse weight were measured three times weekly by caliper measurements. Treatment toxicities were assessed by body weight, decreased food consumption, signs of dehydration, hunching, ruffled fur appearance, inactivity or nonresponsive behavior.

Immunohistochemical and immunofluorescent staining and quantification.

In vitro samples.—The 2D cell lines were seeded in a μ-Slide 8-Well chambered coverslip (ibidi, catalog no. 80826) and treated as previously described. Cells were washed with PBS (Gibco) and fixed with 4% paraformaldehyde for 15 min. After a 5-min PBS wash, cells were permeabilized by the addition of PBS containing 0.25% Triton X-100 for 15 min. After two 5-min washes with PBS, cells were incubated with a blocking solution (1% bovine serum albumin in PBS-T (PBS + 0.1% Tween-20)) for 1 h. Cells were then incubated with diluted primary antibody in blocking solution overnight at 4 °C. After three 5-min PBS washes, cells were incubated with diluted secondary antibody in blocking solution for 1 h at room temperature in the dark. After three 5-min PBS washes, coverslips were imaged using an EVOS FL Auto 2 Cell Imaging System (Thermo Fisher Scientific). The antibodies are given in Supplementary Table 6.

In vivo samples.—For immunohistochemistry (IHC), 4-μm-thick, formalin-fixed, paraffin-embedded sections were prepared using standard sodium citrate antigen-retrieval methods. Primary antibodies were diluted in 1.25% horse serum/PBS and incubated overnight in a humidified chamber at 4 °C overnight. IHC staining was carried out using the ImmPRESS horseradish peroxidase anti-mouse IgG (peroxidase) Polymer Detection Kit (Vector Laboratories) following the manufacturer's instructions for visualization. For immunofluorescence (IF), 4-μm-thick sections were cut from frozen OCT blocks. Tissue sections were fixed in 2% paraformaldehyde for 20 min at room temperature and permeabilized in 0.1% Triton X-100 for 10 min, washed in PBS-T, then blocked for 1 h at room temperature with 5% goat serum + PBS-T. Sections were incubated with primary antibody in a humidified chamber at 4 °C overnight, washed in PBS-T and coverslipped with VECTASHIELD Antifade Mounting Medium with DAPI (Vector Laboratories). The antibodies used are detailed in Supplementary Table 6. For analysis, 20 representative images from each tumor were taken using an EVOS FL Auto 2 Cell Imaging System. Staining intensity was scored using analysis pipelines generated in Image J software[51] (IHC staining) or CellProfiler software[52] (IF staining).

Clinical samples.—Human prostatectomy tissue collection and assessment have been previously described by Calagua et al.[53]. Briefly, scoring was performed semiquantitatively as follows: 0 (negative or <1%), 1 (1–4%), 2 (5–24%), 3 (25–49%) and 4 (≥50%). The antibodies are detailed in Supplementary Table 6. These tissues were stained by IF for detection of dsRNA and H3K27me3. After standard citrate buffer antigen retrieval, sections were incubated with primary antibodies overnight at 4 °C, followed by incubation with a fluorescent conjugated secondary antibody for 1 h at room temperature. For analysis, 100 representative images from tumor regions were taken from each tissue sample using an EVOS FL Auto 2 Cell Imaging System. Staining intensity was quantified as mean pixel intensity per sample using analysis pipelines generated in CellProfiler software[52].

Author Manuscript Author Manuscript Author Manuscript Author Manuscript

Flow cytometry.

In vitro analysis.—The Click-iT EdU Alexa Fluor-488 Flow Cytometry Assay kit (Thermo Fisher Scientific) was used to measure DNA synthesis according to the manufacturer's instructions. For H3K27me3, PD-L1 and dsRNA staining, organoid disks were digested to a single-cell suspension by treatment with TrypLE (Gibco), which was in turn deactivated by resuspension in DMEM (Gibco) supplemented with 10% FBS (Sigma). Cells were washed with PBS (Gibco) by centrifugation at 500*g* and 4 °C, and fixed with 4% paraformaldehyde for 15 min. After another PBS wash, cells were permeabilized by the addition of ice-cold methanol to a final concentration of 90% methanol. This suspension was incubated for 30 min on ice. After two washes with FACS buffer (PBS supplemented with 10% FBS), cells were resuspended in primary antibody prepared in FACS buffer (antibodies detailed in Supplementary Table 6). These cell suspensions were incubated overnight in the dark at 4 °C or for 1 h at room temperature. H3K27me3 and Edu were analyzed using an Amnis ImageStream Mark II (Luminex) and dsRNA and PD-L1 with a BD LSRFortessa (BD Biosciences).

In vivo tumor analysis.—Tumors were disassociated into single-cell suspensions in PBS on ice. Cells were washed with PBS (Gibco) by centrifugation at 500*g* and 4 °C, and fixed with 4% paraformaldehyde for 15 min. After another PBS wash, cells were permeabilized by the addition of ice-cold methanol to a final concentration of 90% methanol and incubated for 30 min on ice. After two washes with FACS buffer (5% FBS/PBS), cells were resuspended in primary antibody prepared in FACS buffer. These cell suspensions were incubated at 4 °C or for 1 h at room temperature, protected from light. Cells were washed twice in FACS buffer and analyzed on a BD LSRFortessa, separated into 'CD45^{-}' and 'CD45^{+}' events. The antibodies used are given in Supplementary Table 6.

In vivo tumor immune profiling.—Tumor cell suspensions were stained using two different antibody panels: lymphocytes or myeloid, using appropriate IgG and full minus one controls, followed by analysis on an LSRII flow cytometer (BD Biosciences). Antibodies for the various immune panels are as follows: lymphocyte panel (Ghost Dye Red 780, anti-human CD8 (dump channel), anti-mouse CD3, anti-mouse CD4, anti-mouse CD8, anti-mouse CD45 and anti-mouse PD-1); and myeloid panel (Ghost Dye Red 780, anti-human CD8, anti-mouse CD11b, anti-mouse CD45, anti-mouse Ly6C, anti-mouse Ly6G and anti-mouse I-A/I-E). After surface staining, fixation and permeabilization (BD Cytofix and BD Cytoperm), cells were stained for the following intracellular markers: lymphocyte panel (Foxp3, Ki67 or the appropriate IgG controls). After staining, cells were analyzed on an LSRII flow cytometer (BD Biosciences). Cells were gated based on singlets, size/nucleation, Ghost Dye Red 780-negative events and dump-negative events ('Live events'). Cells were then separated into CD45^{-} and CD45^{+} events, and immune populations were defined as follows: CD3^{+}CD4^{+} T cells, CD3^{+}CD8^{+} T cells, CD3^{+}CD4^{+}Foxp3^{+} T_{reg} cells, granulocytic MDSCs (CD11b^{+}MHC-II^{-}Ly6C^{lo} Ly6G^{+}) and monocytic MDSCs (CD11b^{+}MHC-II^{-}Ly6G^{-}Ly6C^{hi}). The antibodies used are detailed in Supplementary Table 6.

Author Manuscript Author Manuscript Author Manuscript Author Manuscript

RT–qPCR.

The qPCRs were performed in accordance with MIQE guidelines[54]. RNA was harvested using a standard TRIzol protocol according to the manufacturer's instructions. Complementary DNA was synthesized using the qScript cDNA SuperMix (Quantabio), according to the manufacturer's instructions. The SsoAdvanced Universal SYBR Green Supermix (Bio-Rad) was used for PCRs with the cycling conditions recommended in the manufacturer's instructions. The primers used are detailed in Supplementary Table 7.

Sequencing analysis.

RNA-seq data generation.—EMC mouse organoids were seeded at a concentration of 20,000 cells per 40 μl of Matrigel disk (1 disk per well of a 24-well plate) and treated with 5 μM DZNep, DMSO control, 1 μM Tam or ethanol control for 3 d. RNA was harvested from samples using TRIzol (Thermo Fisher Scientific) according to the manufacturer's instructions. RNA libraries were prepared with the TruSeq stranded messenger RNA sample preparation kits (Illumina) from 500 ng of purified total RNA, according to the manufacturer's protocol. The resultant RNA dsDNA libraries were quantified by Qubit fluorometer, Agilent TapeStation 2200 and RT–qPCR using the Kapa Biosystems library quantification kit according to the manufacturer's protocols. Uniquely indexed libraries were pooled in equimolar ratios and sequenced on a single NextSeq 500 Sequencing Platform (Illumina) run with single-end 75-bp reads. Sequencing reads were aligned to the UCSC mm9 reference genome assembly and gene counts were quantified using STAR (v.2.5.1b)[55] and normalized read counts (reads per kilobase per million) were calculated using Cufflinks (v.2.2.1)[56].

EZH2 repression score.—DE gene analysis and GSEA were first performed using RNA-seq data obtained from EMC mouse 3D organoids treated with DZNep ($n = 3$) and EMC mouse 3D organoids treated with the DMSO vehicle ($n = 3$). DZNep versus DMSO RNA-seq data were used to generate a 29-gene signature, which contained the most DE genes with human homologs. Weights were again defined as the $-\log_{10}$ of the adjusted P value multiplied by the sign of the $\log_2$(fold-change). The EZH2 repression score was generated for each tumor sample by multiplying the log(transformed count data) for each of the 29 human orthologous genes, using its established weighting and summing these 29 values for each sample.

ChIP–seq and ATAC–seq of patient samples.—Fresh–frozen radical prostatectomy specimens from patients with localized PCa were obtained from the Dana-Farber Cancer Institute Gelb Center biobank, under Dana-Farber Cancer Institute/Harvard Cancer Center IRB-approved protocols (nos. 01–045, 09–171). Hematoxylin and eosin (H&E)-stained slides from each case were reviewed by a genitourinary pathologist. Areas estimated to be enriched >70% for prostate tumor tissue were isolated for analysis. ChIP–seq was performed using the protocol previously described[27] with antibodies to H3K27Ac (Diagenode, catalog no. C15410196) and H3K27me3 (Cell Signaling Technology, catalog no. 9733S). Libraries were sequenced using 75-bp reads on the Illumina platform. ATAC–seq (assay for transposase-accessible chromatin with high-throughput sequencing) was performed at Active Motif using fresh–frozen Gelb Center RP tumor and normal epithelium specimens.

Author Manuscript Author Manuscript Author Manuscript Author Manuscript

The tissue was manually disassociated, isolated nuclei were quantified using a hemocytometer and 100,000 nuclei were tagmented as previously described[57], with some modifications[58] using the enzyme and buffer provided in the Nextera Library Prep Kit (Illumina). Tagmented DNA was then purified using the MinElute PCR purification kit (QIAGEN), amplified with ten cycles of PCR and purified using Agencourt AMPure SPRI beads (Beckman Coulter). All samples were processed through the computational pipeline developed at the DFCI Center for Functional Cancer Epigenetics (CFCE) using primarily open-source programs. Sequence tags were aligned with the Burrows–Wheeler aligner (BWA) to build hg19 of the human genome, and uniquely mapped, nonredundant reads were retained[59]. These reads were used to generate binding sites with Model-Based Analysis of ChIP–seq 2 (MACS v.2.1.1.20160309), with a *q* value (false discovery rate threshold of 0.01 (ref.[60])). The ChIP–seq and ATAC–seq data are reported separately[28].

ENV sequence identification.—Fastq files were downloaded from the ENA public repository (https://www.ebi.ac.uk/ena/browser/view/PRJNA421359). ChIP–seq fastq files were processed using GenPipes 'ChIPseq' pipeline steps 1–8 (ref.[61]). In brief, raw reads are trimmed and filtered for quality using Trimmomatic and then mapped to the human reference genome (GRCh38) using the BWA to generate Bam files. Peaks were then called using MACS2 software (v.2.1.2)[60] with default setting. Generated bed files were further analyzed using R environment (v.3.6.2). The findOverlappingPeaks-function from the ChIPpeakAnno_3.20.1 package[62] was used to identify overlapping peaks. Peaks were annotated according to genomic location and closest gene using the ChIPseeker_1.22.1 package[63] and the reference genome annotation package TxDb.Hsapiens.UCSC.hg38.knownGene_3.10.0. The list of peaks that lost H3K27 trimethylation on EZH2 knockdown were generated by overlapping LNCaP siCtrl H3K27me3 peaks with LNCaP siEZH2 H3K27me3 peaks. The list of peaks that gained H3K27 acetylation on EZH2 knockdown was generated by overlapping LNCaP siCtrl H3K27ac peaks with LNCaP siEZH2 H3K27ac peaks. To generate the list of genes with 3′-UTR, we followed the procedure described in Canadas et al.[23]. The 5,880 3′-UTRs that have ERVs were subset to keep only unique gene symbols. We then intersected this list of 2,137 genes to the closest genes with peaks that lost methylation and gained acetylation.

Statistics and reproducibility.

The sample size was based on the number of samples available for computational analysis of human samples. For mouse RNA-seq analysis, chemical and genetic inhibition of Ezh2 was performed in triplicate and duplicate, respectively. No statistical method was used to predetermine sample size and experiments were not randomized. The investigators were blinded for in vivo therapy experiments because one person conducted treatment and an independent person recorded tumor measurements. For analysis of all IHC and IF staining (clinical samples and in vivo tumor samples), the slides were coded before analysis to blind researchers to treatment groups and scored digitally to prevent potential bias. For in vitro experiments, blinding was not possible because the same researchers who treated the cells ran the analysis. However, all analysis within experiments was run at the same time in an automated manner, so prior knowledge of treatment groups had no impact on data output. There was no data exclusion from any experiment in our analysis.

Author Manuscript Author Manuscript Author Manuscript Author Manuscript

For RNA-seq analysis of mouse and human datasets, DE gene analysis, sample-to-sample distance calculations and principal component analysis were conducted using the DESeq2 package in R. Raw RNA-seq count data were processed to remove genes lacking expression in >80% of samples. Low count genes, with fewer than ten total reads, were also filtered out. After variance-stabilizing transformation, a Euclidean sample distance matrix and principal component plots were generated to compare global gene expression profiles between samples. DE gene lists were then generated. Further interpretation of gene expression data was enabled using GSEA. A ranked list was generated from the DE gene output by multiplying the $-\log_{10}$ of the adjusted P value by the sign of the $\log_2$(fold-change). The ranked list was then used as an input to the GSEA preranked tool to generate enrichment scores using the Hallmark, Curated and Oncogenic Signatures gene sets in the Molecular Signatures Database. Heatmaps and unsupervised hierarchical cluster analysis, using Euclidean distance measurements, were performed using the pheatmaps package in R. The corr. test and smoothScatter functions were used for Pearson's correlation analysis and to generate scatter plots. The VennDiagram package was used to compare gene lists and generate Venn diagrams. Master regulator analysis was performed using MARINa[64]. Protein association network generation and Gene Ontology analyses were performed using STRING v.11 (ref.[65]).

In vitro experiments were conducted in three independent experiments and displayed as mean ± s.e.m. For in vivo experiments, ten animals were used per treatment group following our previous studies. Graph preparation and statistical analyses of in vitro and in vivo experiments were performed using GraphPad Prism software. Statistical significance for assays was assessed using either a one-way analysis of variance (ANOVA), Tukey's multiple-comparison test or Welch's corrected unpaired Student's *t*-test unless otherwise stated. Specific for in vivo tumor growth curves (Fig. 4b), a multiple Student's *t*-test was used to assess therapy response. An observation with a $P < 0.05$ was considered to be statistically significant.

Reporting Summary.

Further information on research design is available in the Nature Research Reporting Summary linked to this article.

Data availability

ChIP–seq, ATAC–seq and RNA-seq data used to support the present study have been deposited in the Gene Expression Omnibus under accession nos. GSE130408, GSE107780, GSE146617 and GSE146076. Further information and requests for resources and reagents should be directed to the lead author, L.E. (Leigh.Ellis@cshs.org). Gene expression data for LNCaP cell lines treated with EZH2 inhibitor were obtained under accession no. GSE107780. Raw and normalized expression data for 550 TCGA PCa samples were obtained from the NCI Genomic Data Commons Data Portal. Some 102 samples were excluded based on pathological criteria provided by S. Tyekucheva and M. Loda, and the remaining 448 samples (40 normal samples and 408 tumor samples) were included in subsequent analyses. The NCI data were provided by A. Sowalsky. Human PCas have been

described previously[66] and were obtained from DbGaP (study accession no. phs000909). Normalized counts from the Stand Up 2 Cancer dataset were obtained from cBioPortal[67]. Any code used in this manuscript will be made available upon request. Source data are provided with this paper.

Extended Data

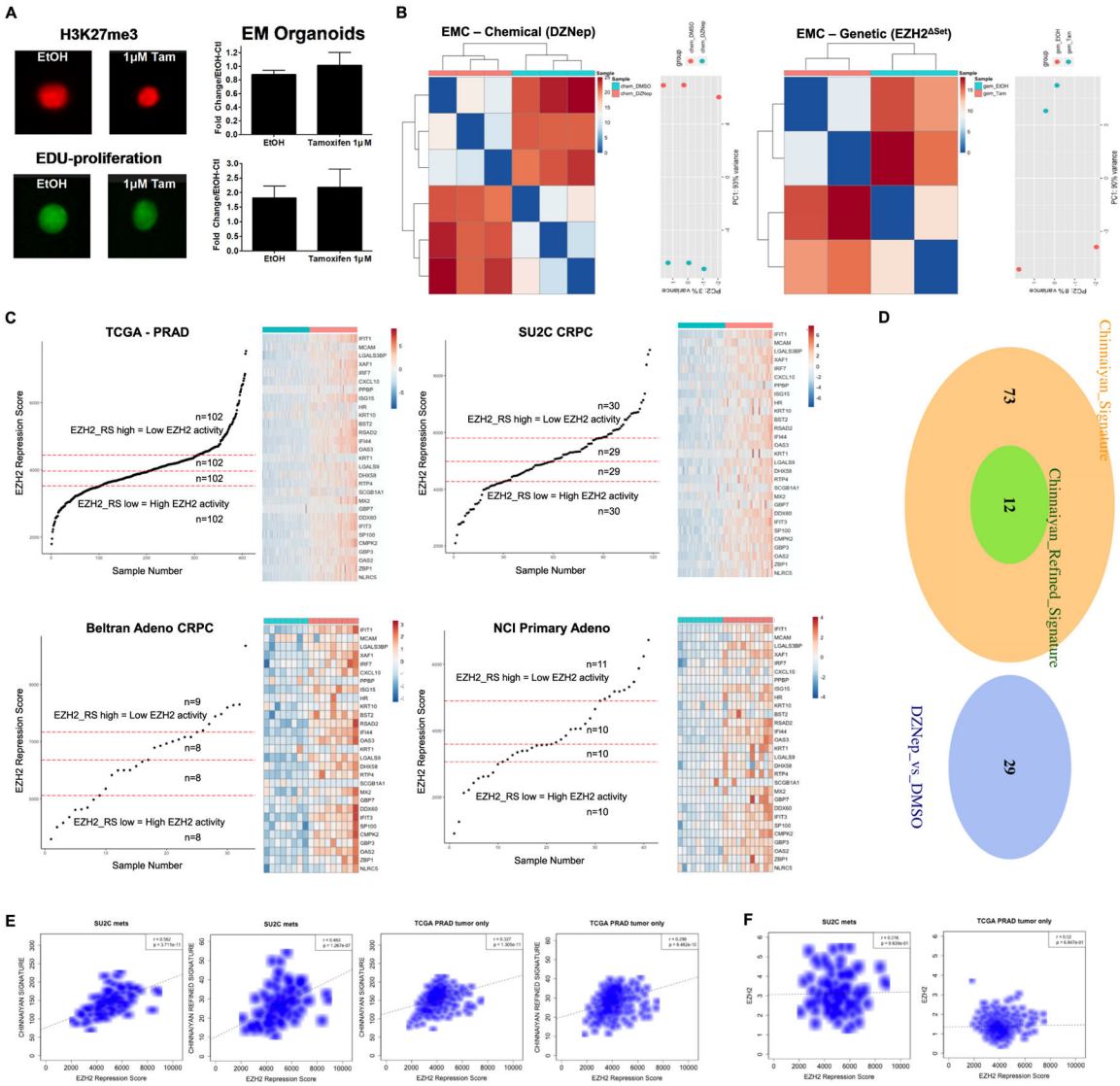

Extended Data Fig. 1 |. Generation of an EZH2 Activity Gene Signature.

(a) Three-dimensional PCa organoids generated from EM mice (without PSACre^{ERT2}) alleles. When treated with tamoxifen, no loss of H3K27me3 or EDU staining is indicated - demonstrating specificity of tamoxifen-PSACre^{ERT2} mediated deletion of the Ezh2 set domain in Fig. 1. P-values were generated using a two-tailed unpaired T-test with Welch's correction. Data was generated from three (n = 3) independent experiments and displayed as mean ±SEM **(b)** Principal component analysis (PCA) following chemical (n = 3 independent organoid cultures per treatment group) and genetic (n = 2 independent organoid cultures per

Author Manuscript Author Manuscript Author Manuscript Author Manuscript

Author Manuscript Author Manuscript Author Manuscript Author Manuscript

treatment group) inhibition of Ezh2 catalytic function results in significant changes in gene expression. **(c)** A 29-gene signature derived from Fig. 1c (DZNep data) was used to generate signature scores for each patient within four independent human prostate cancer RNA-seq datasets. Patients were ranked highest score to lowest score and subject to quartile separation. First (blue) and fourth (red) quartiles were analyzed by supervised clustering to demonstrate expression differences within patients with lowest EZH2 activity and highest EZH2 activity. Sample numbers used for TCGA (n = 408 samples), SU2C (n = 118 samples), Beltran Adenocarcinomas (n = 33 samples), and NCI Primary Adeno (n = 41 samples). **(d)** Our 29-gene signature derived from demonstrates complete independence from a previously published polycomb repression signature. **(e)** Our 29 gene signature demonstrates significant correlation with a previously published polycomb repression signature in 2 independent human PCa gene expression datasets. **(f)** EZH2 activity is not determined by EZH2 mRNA expression. Pearson correlation coefficient analysis was utilized to generate data for E-F.

Author Manuscript Author Manuscript Author Manuscript Author Manuscript

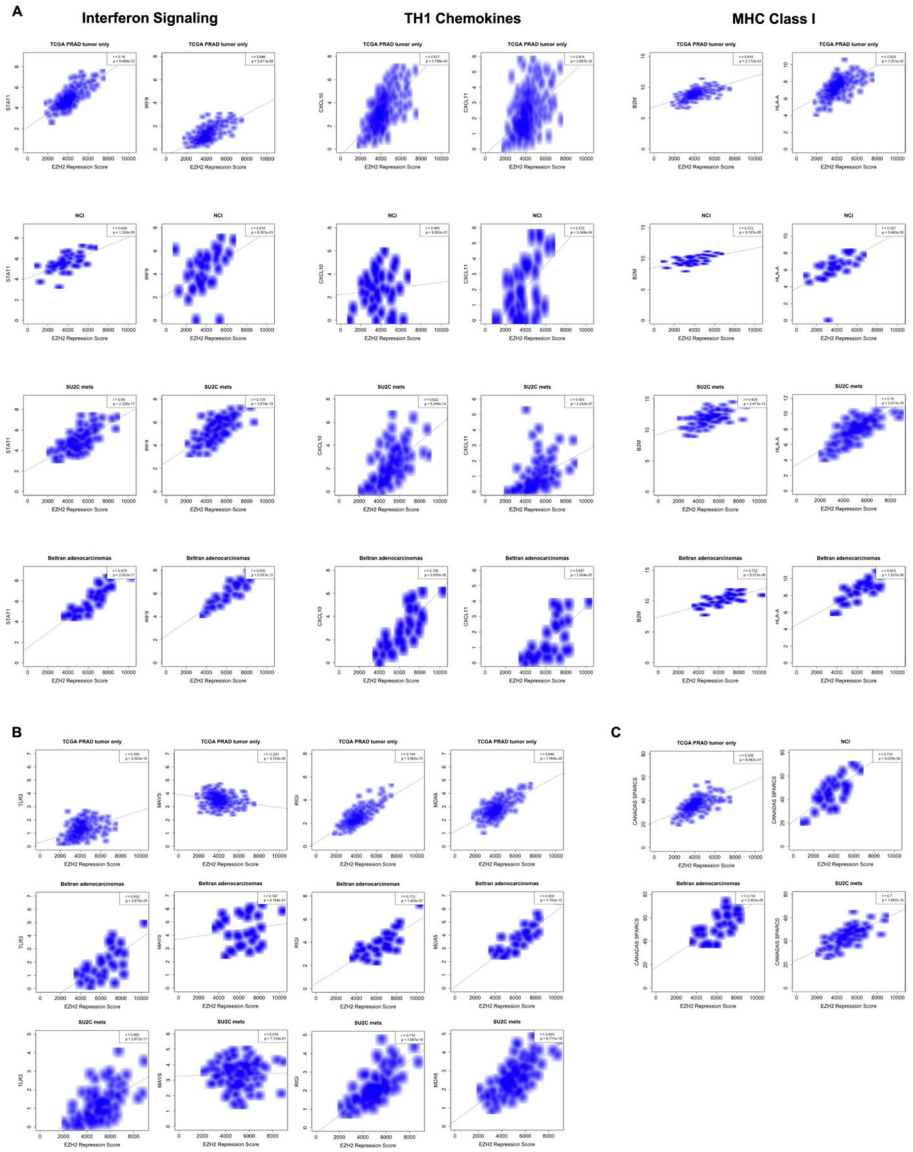

Extended Data Fig. 2 |. Low EZH2 Activity is Associated with Enrichment in IFN Signaling and dsRNA Sensory Machinery.

(a) Genes representing IFN signaling (*STAT1, IRF9*), Th1 chemokines (*CXCL10, CXCL11*), and MHC Class I molecules (*B2M, HLA-A*) were shown to be enriched in PCa patients with low EZH2 activity. **(b)** Genes representing intracellular sensors of dsRNA (*TLR3, MAVs, RIG-I, MDA5*) were shown to be enriched in PCa patients with low EZH2 activity. **(c)** Genes from Canadas et al. (2018) described as 'SPARCs' regulated by STAT1 and EZH2 that house endogenous retroviral sequences important for inducing an innate immune response, were shown to be enriched in PCa patients with low EZH2 activity. Sample numbers used for TCGA (n = 408 samples), SU2C (n = 118 samples), Beltran Adenocarcinomas (n = 33 samples), and NCI Primary Adeno (n = 41 samples). All data was generated by using Pearson correlation coefficient analysis.

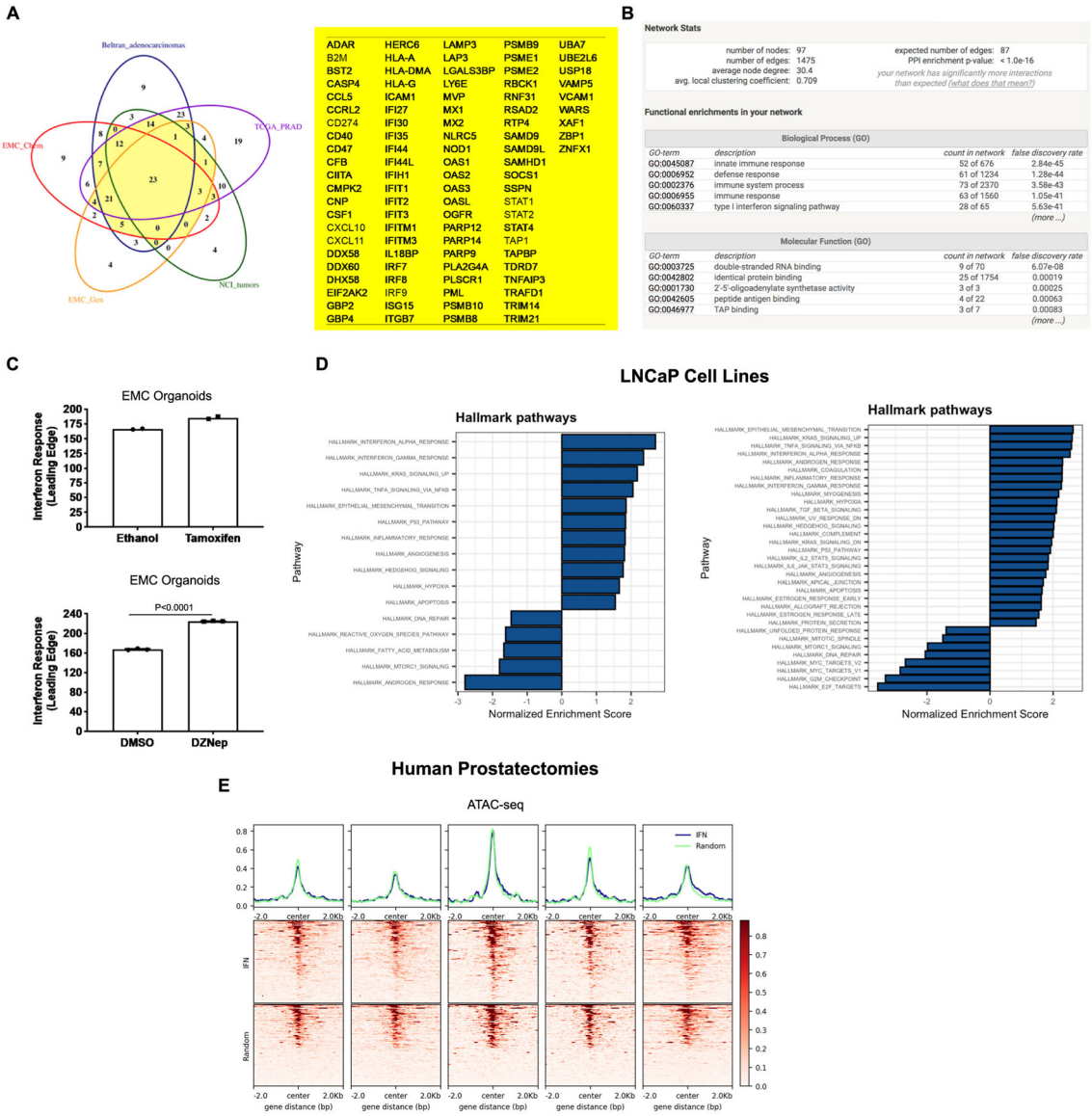

Extended Data Fig. 3 |. EZH2 Inhibition Regulates Innate Immune Signaling in Prostate Cancer. **(a)** Overlay of five independent differentially expressed IFNα and IFNγ gene lists from mouse and human RNA-seq data provided a merged gene list of 97 ISGs. **(b)** String analysis of the generated 97 type I/II IFN gene list reveals significant enrichment of biological processes including *innate immune response*, *defense response*, and *type I interferon signaling pathway*. Moreover, molecular function terms including *double-stranded RNA binding*, *peptide antigen binding* were also significantly enriched. **(c)** Mouse RNA-seq data was queried to demonstrate that our 97 IFN gene signature is upregulated in response to loss of EZH2 catalytic activity. Data was generated by performing two (n = 2) independent (genetic inhibition) or three (n = 3) independent experiments and displayed as the mean or mean ±SEM respectively. Statistical data was generated by performing a two-tailed unpaired T-test with Welch's correction. **(d)** LNCaP RNA-seq data was queried to demonstrate that upon EZH2 genetic (left) or chemical (right) inhibition results in enrichment of IFNα/γ

Author Manuscript Author Manuscript Author Manuscript Author Manuscript

gene sets. Data was generated from previously published RNA-seq data – GSE107780. Triplicate, n = 3/treatment group RNA-seq experiments where available for analysis. **(e)** Heatmaps of normalized ATAC signal intensities of 97 ISGs from were analyzed in 5 independent patient prostatectomy samples. Each patient sample was analyzed once.

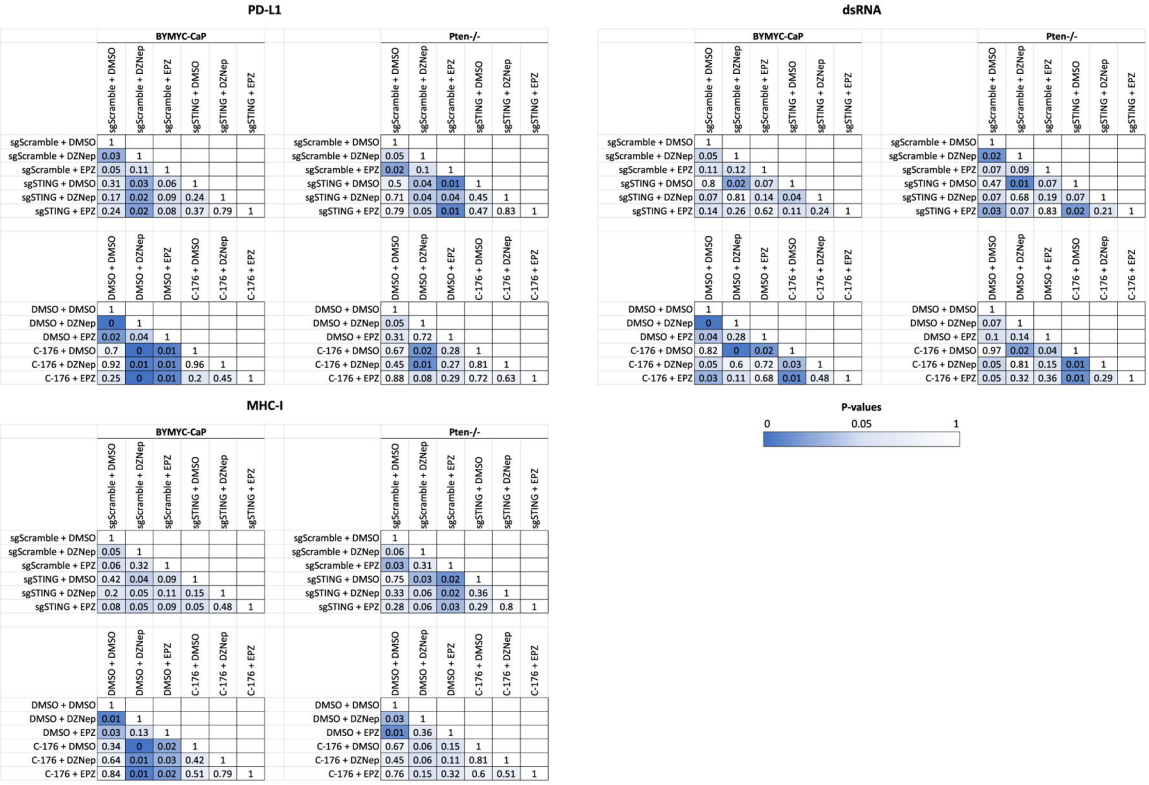

Extended Data Fig. 4 |. Activation of interferon stimulated genes is STING dependent cont. Full statistical comparisons for flow cytometry analysis of PD-L1, MHC-I and dsRNA expression in B6MYC-CaP and Pten−/− cells with and without STING inhibition (chemical by C-176 or genetic by sgSTING) and treated with DMSO, or EZH2 inhibitors DZNep or EPZ. These statistical data are partnered with Fig. 4c,d and was generated by performing a two-tailed unpaired T-test with Welch's correction. Data was generated using flow cytometry analysis from three (n = 3) independent experiments and displayed as mean ±SEM. P-values can be seen in Extended Data Fig. 4 and were generated using a two-tailed unpaired T-test with Welch's correction. Note: Data from Pten KO cells in Fig. 4c treated with C176 to inhibit STING was generated from two (n = 2) independent experiments and displayed as the mean value.

Author Manuscript Author Manuscript Author Manuscript Author Manuscript

Author Manuscript Author Manuscript Author Manuscript Author Manuscript

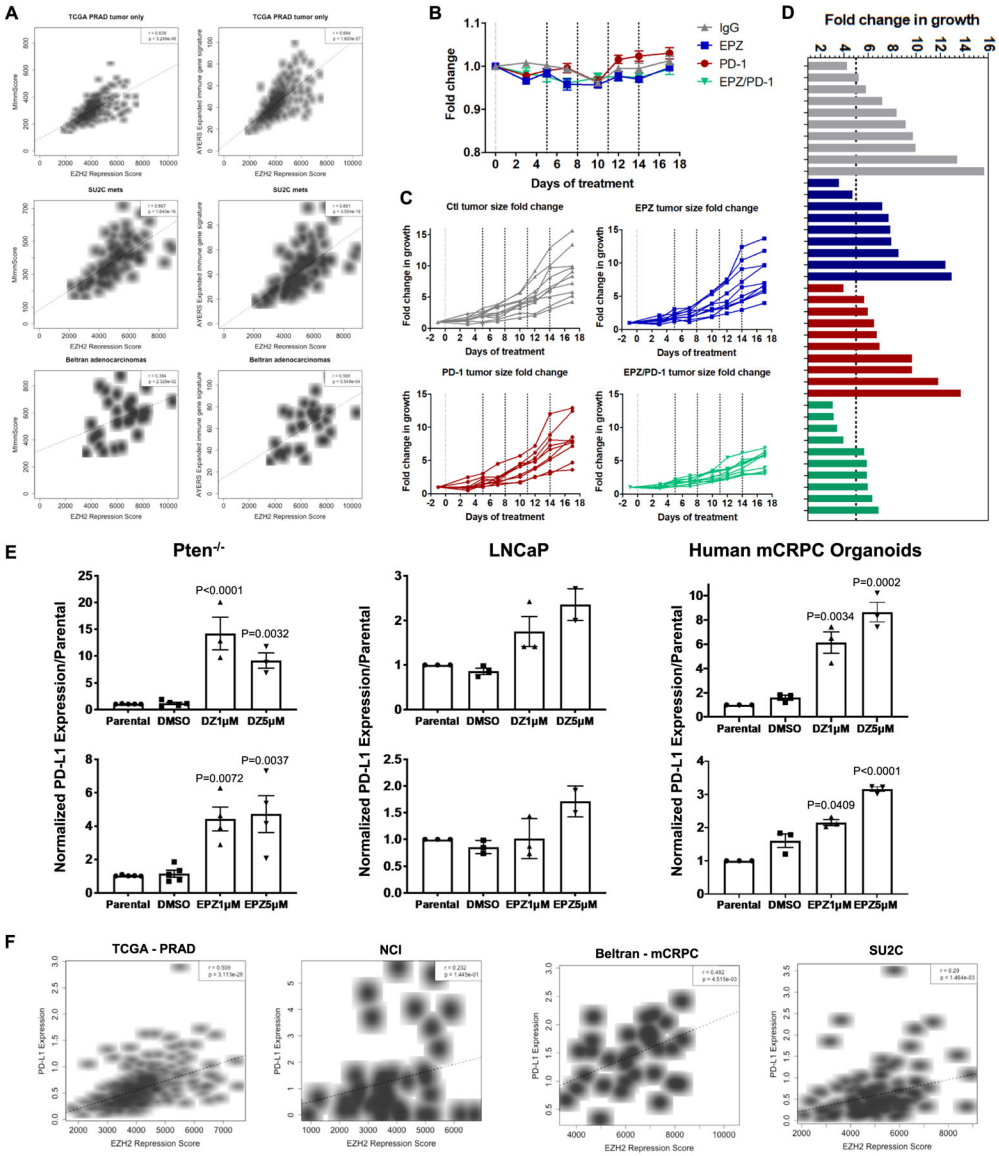

Extended Data Fig. 5 |. Low EZH2 activity is associated with increased immune gene expression related to positive response to check-point inhibition.

(**a**) Analysis of human RNA-seq datasets reveal immune signatures related to check-point blockade positive response are significantly enriched in PCa patients with low EZH2 activity. Sample numbers used for TCGA (n = 408 samples), SU2C (n = 118 samples), and Beltran Adenocarcinomas (n = 33 samples). (**b**) Normalized weights of mice (n = 10 mice/treatment group) indicate that no significant weight loss (ie: toxicity) was observed following therapy with indicated treatment cohorts. (**c-d**) Tumor measurements of individual tumors by waterfall or spider plots validate significant anti-tumor activity of EZH2 inhibition combined with PD-1 blockade. N = 10 mice/tumors per treatment group. (**e**) Mouse and human prostate cancer organoids (Pten−/− and human mCRPC organoids), and human LNCaP 2D cell lines treated with indicated EZH2 inhibitors for 96 hours demonstrate upregulation of PD-L1 mRNA. Data was generated for Pten−/− organoids with n = 5 independent experiments for parental and DMSO treatment groups and n = 3

independent experiments for DZ and EPZ treatment groups and displayed as the mean ±SEM. For LNCaP and human CRPC organoids, a n = 3 independent experiment was used to generate data and displayed as the mean ±SEM. Statistical data was generated by performing a two-tailed unpaired T-test with Welch's correction of DMSO verse DZ or EPZ treatment groups. (**f**) Human PCa gene expression data was queried to demonstrate that increased PD-L1 gene up-regulation is significantly correlated with low EZH2 activity. Sample numbers used for TCGA (n = 408 samples), NCI (n = 41 samples), SU2C (n = 118 samples), and Beltran Adenocarcinomas (n = 33 samples).

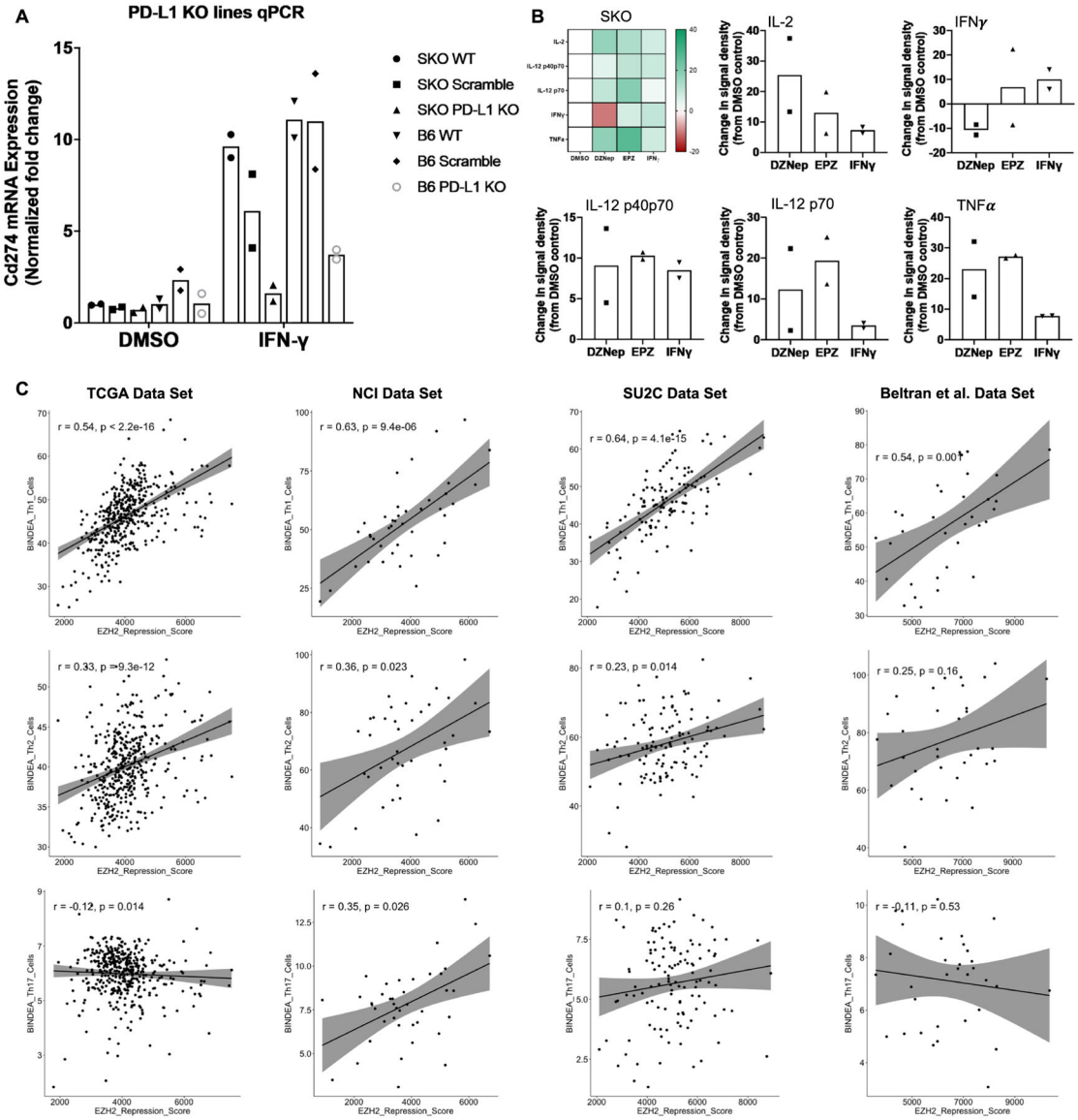

Extended Data Fig. 6 |. Low EZH2 activity is associated with positive association of inflammatory immune genes.

(**a**) B6MYC-CaP and Pten−/− 2D cell lines that express Cas9 were stably infected with gRNA towards *Pd-l1* (*Cd274*). Treatment with IFNγ validates the inhibition of *Pd-l1* expression in KO cell lines. Data was generated by n = 2 independent qRT-PCR

Author Manuscript Author Manuscript Author Manuscript Author Manuscript

Author Manuscript Author Manuscript Author Manuscript Author Manuscript

experiments. (**b**) Murine Pten KO prostate cancer cells treated with EZH2 inhibitors increase expression of Th-1 cytokines. Data for A-B was generated by performing two (n = 2) independent experiments and displayed as the mean. (**c**) Human prostate cancer patient correlation analysis between EZH2 repression score (X-axis) and Th1, Th2, or Th17 gene expression profiles (Y-axis). Sample numbers used for TCGA (n = 408 samples), NCI (n = 41 samples), SU2C (n = 118 samples), and Beltran Adenocarcinomas (n = 33 samples).

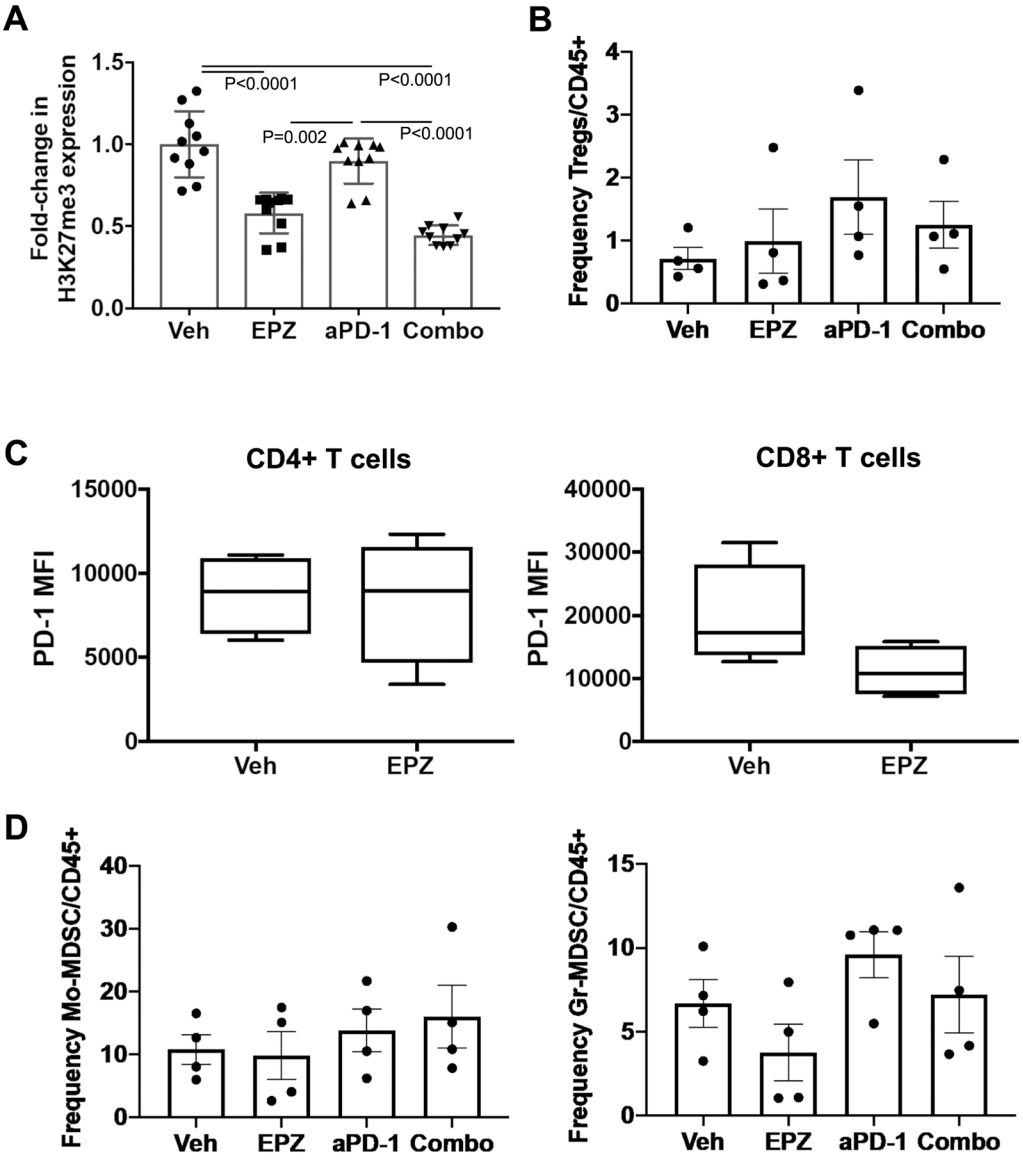

Extended Data Fig. 7 |. Effects on the tumor microenvironment post EZH2 inhibition.
(**a**) Representative in vivo tumor analysis indicates that EZH2 inhibition and combination significantly reduce tumor H3K27me3 expression. (**b**) Frequency of Foxp3 + T-reg cells was determined by flow cytometry. No significant change was observed following treatment. (**c**) PD-1 protein expression on CD4 + and CD8 + T-cells was analyzed by flow cytometry. Only CD8 + T-cells were observed to express lower PD-1 protein following EZH2 inhibition. Box

Author Manuscript Author Manuscript Author Manuscript Author Manuscript

plots are displayed as min to max distribution. (**d**) Frequency of Mo-MDSC and Gr-MDSC cells was determined by flow cytometry. No significant change was observed following treatment. Data was generated by analysis of (A) ten (n = 10) independent mice or (B-D) four (n = 4) independent mice per treatment group. Statistical data was generated by performing a two-tailed unpaired T-test with Welch's correction.

Supplementary Material

Refer to Web version on PubMed Central for supplementary material.

Acknowledgements

The present study was supported by Dana-Farber Cancer Institute Faculty Start-Up Funds (to L.E.), a Prostate Cancer Foundation Young Investigator Award (to L.E., D.P.L., S.W. and A.G.S.) and the Intramural Research Program of the National Institutes of Health, National Cancer Institute (NCI; to A.G.S.). B.M.O was supported by Emory University Faculty Start-Up funds. D.P.L. is a Lewis Katz recipient of a Scholarship for the Next Generation of Scientists from the Cancer Research Society, and is also a Research Scholar, Junior 1 of the Fonds de la recherche du Québec-Santé. This research project was supported in part by the Emory University School of Medicine Flow Cytometry Core (to B.M.O.). We thank Epizyme Pharmaceuticals for supplying EPZ0011989. The results shown here are in whole or part based on data generated by the TCGA Research Network: https://www.cancer.gov/tcga.

References

1. Siegel RL, Miller KD & Jemal A Cancer statistics, 2019. CA Cancer J. Clin 69, 7–34 (2019). [PubMed: 30620402]
2. Gan L et al. Epigenetic regulation of cancer progression by EZH2: from biological insights to therapeutic potential. Biomark Res. 6, 10 (2018). [PubMed: 29556394]
3. Varambally S et al. The polycomb group protein EZH2 is involved in progression of prostate cancer. Nature 419, 624–629 (2002). [PubMed: 12374981]
4. Koh CM et al. Myc enforces overexpression of EZH2 in early prostatic neoplasia via transcriptional and post-transcriptional mechanisms. Oncotarget 2, 669–683 (2011). [PubMed: 21941025]
5. Peng D et al. Epigenetic silencing of TH1-type chemokines shapes tumour immunity and immunotherapy. Nature 527, 249–253 (2015). [PubMed: 26503055]
6. Ennishi D et al. Molecular and genetic characterization of MHC deficiency identifies EZH2 as therapeutic target for enhancing immune recognition. Cancer Discov. 9, 546–563 (2019). [PubMed: 30705065]
7. Burr ML et al. An evolutionarily conserved function of polycomb silences the MHC class I antigen presentation pathway and enables immune evasion in cancer. Cancer Cell 36, 385–401 e388 (2019). [PubMed: 31564637]
8. Roulois D et al. DNA-demethylating agents target colorectal cancer cells by inducing viral mimicry by endogenous transcripts. Cell 162, 961–973 (2015). [PubMed: 26317465]
9. Nagarsheth N et al. PRC2 epigenetically silences Th1-type chemokines to suppress effector T-cell trafficking in colon cancer. Cancer Res. 76, 275–282 (2016). [PubMed: 26567139]
10. Sheng W et al. LSD1 ablation stimulates anti-tumor immunity and enables checkpoint blockade. Cell 174, 549–563 e519 (2018). [PubMed: 29937226]
11. Stone ML et al. Epigenetic therapy activates type I interferon signaling in murine ovarian cancer to reduce immunosuppression and tumor burden. Proc. Natl Acad. Sci. USA 114, E10981–E10990 (2017). [PubMed: 29203668]
12. Zingg D et al. The histone methyltransferase Ezh2 controls mechanisms of adaptive resistance to tumor immunotherapy. Cell Rep. 20, 854–867 (2017). [PubMed: 28746871]
13. Adeegbe DO et al. Synergistic immunostimulatory effects and therapeutic benefit of combined histone deacetylase and bromodomain inhibition in non-small cell lung cancer. Cancer Discov. 7, 852–867 (2017). [PubMed: 28408401]

Author Manuscript Author Manuscript Author Manuscript Author Manuscript

14. Hogg SJ et al. BET-bromodomain inhibitors engage the host immune system and regulate expression of the immune checkpoint ligand PD-L1. Cell Rep. 18, 2162–2174 (2017). [PubMed: 28249162]
15. Wee ZN et al. EZH2-mediated inactivation of IFN-gamma-JAK-STAT1 signaling is an effective therapeutic target in MYC-driven prostate cancer. Cell Rep. 8, 204–216 (2014). [PubMed: 24953652]
16. Johnson ML et al. Preliminary results of ENCORE 601, a phase 1b/2, open-label study of entinostat (ENT) in combination with pembrolizumab (PEMBRO) in patients with non-small cell lung cancer (NSCLC). J. Clin. Oncol 34, e20659–e20659 (2016).
17. Ellis L et al. Generation of a C57BL/6 MYC-driven mouse model and cell line of prostate cancer. Prostate 76, 1192–1202 (2016). [PubMed: 27225803]
18. Xie H et al. Polycomb repressive complex 2 regulates normal hematopoietic stem cell function in a developmental-stage-specific manner. Cell Stem Cell 14, 68–80 (2014). [PubMed: 24239285]
19. Ratnacaram CK et al. Temporally controlled ablation of PTEN in adult mouse prostate epithelium generates a model of invasive prostatic adenocarcinoma. Proc. Natl Acad. Sci. USA 105, 2521–2526 (2008). [PubMed: 18268330]
20. Zou W, Wolchok JD & Chen L PD-L1 (B7-H1) and PD-1 pathway blockade for cancer therapy: mechanisms, response biomarkers, and combinations. Sci. Transl. Med 8, 328rv324 (2016).
21. Yu J et al. A polycomb repression signature in metastatic prostate cancer predicts cancer outcome. Cancer Res. 67, 10657–10663 (2007). [PubMed: 18006806]
22. Jones PA, Ohtani H, Chakravarthy A & De Carvalho DD Epigenetic therapy in immune-oncology. Nat. Rev. Cancer 19, 151–161 (2019). [PubMed: 30723290]
23. Canadas I et al. Tumor innate immunity primed by specific interferon-stimulated endogenous retroviruses. Nat. Med 24, 1143–1150 (2018). [PubMed: 30038220]
24. Li H et al. Immune regulation by low doses of the DNA methyltransferase inhibitor 5-azacitidine in common human epithelial cancers. Oncotarget 5, 587–598 (2014). [PubMed: 24583822]
25. Chiappinelli KB et al. Inhibiting DNA methylation causes an interferon response in cancer via dsRNA including endogenous retroviruses. Cell 164, 1073 (2016). [PubMed: 27064190]
26. Kim J et al. Polycomb- and methylation-independent roles of EZH2 as a transcription activator. Cell Rep. 25, 2808–2820 e2804 (2018). [PubMed: 30517868]
27. Pomerantz MM et al. The androgen receptor cistrome is extensively reprogrammed in human prostate tumorigenesis. Nat. Genet 47, 1346–1351 (2015). [PubMed: 26457646]
28. Pomerantz MM et al. Prostate cancer reactivates developmental epigenomic programs during metastatic progression. Nat. Genet 52, 790–799 (2020). [PubMed: 32690948]
29. Robinson DR et al. Integrative clinical genomics of metastatic cancer. Nature 548, 297–303 (2017). [PubMed: 28783718]
30. Ayers M et al. IFN-gamma-related mRNA profile predicts clinical response to PD-1 blockade. J. Clin. Invest 127, 2930–2940 (2017). [PubMed: 28650338]
31. Bindea G et al. Spatiotemporal dynamics of intratumoral immune cells reveal the immune landscape in human cancer. Immunity 39, 782–795 (2013). [PubMed: 24138885]
32. Su W et al. The polycomb repressor complex 1 drives double-negative prostate cancer metastasis by coordinating stemness and immune suppression. Cancer Cell 10.1016/j.ccell.2019.06.009 (2019).
33. Rexer H, Graefen M, Merseburger A & AUO. Phase II study of pembrolizumab (MK-3475) in patients with metastatic castration-resistant prostate cancer (KEYNOTE-199)-study AP 93/16 of the AUO. (In German) Urologe A 56, 1471–1472 (2017). [PubMed: 28980011]
34. Rodrigues DN et al. Immunogenomic analyses associate immunological alterations with mismatch repair defects in prostate cancer. J. Clin. Invest 128, 5185 (2018).
35. Wu YM et al. Inactivation of CDK12 delineates a distinct immunogenic class of advanced prostate cancer. Cell 173, 1770–1782.e1714 (2018). [PubMed: 29906450]
36. Zhang J et al. Cyclin D-CDK4 kinase destabilizes PD-L1 via cullin 3-SPOP to control cancer immune surveillance. Nature 553, 91–95 (2018). [PubMed: 29160310]

Author Manuscript Author Manuscript Author Manuscript Author Manuscript

37. Calcinotto A et al. IL-23 secreted by myeloid cells drives castration-resistant prostate cancer. Nature 559, 363–369 (2018). [PubMed: 29950727]
38. Wang D et al. Targeting EZH2 reprograms intratumoral regulatory T cells to enhance cancer immunity. Cell Rep 23, 3262–3274 (2018). [PubMed: 29898397]
39. Tumes DJ et al. The polycomb protein Ezh2 regulates differentiation and plasticity of $CD4^+$ T helper type 1 and type 2 cells. Immunity 39, 819–832 (2013). [PubMed: 24238339]
40. Soshnev AA, Josefowicz SZ & Allis CD Greater than the sum of parts: complexity of the dynamic epigenome. Mol. Cell 69, 533 (2018).
41. Goswami S et al. Modulation of EZH2 expression in T cells improves efficacy of anti-CTLA-4 therapy. J. Clin. Invest 128, 3813–3818 (2018). [PubMed: 29905573]
42. de Groot AE & Pienta KJ Epigenetic control of macrophage polarization: implications for targeting tumor-associated macrophages. Oncotarget 9, 20908–20927 (2018). [PubMed: 29755698]
43. Wang S et al. Prostate-specific deletion of the murine Pten tumor suppressor gene leads to metastatic prostate cancer. Cancer Cell 4, 209–221 (2003). [PubMed: 14522255]
44. Wu X et al. Generation of a prostate epithelial cell-specific Cre transgenic mouse model for tissue-specific gene ablation. Mech. Dev 101, 61–69 (2001). [PubMed: 11231059]
45. Shen X et al. EZH1 mediates methylation on histone H3 lysine 27 and complements EZH2 in maintaining stem cell identity and executing pluripotency. Mol. Cell 32, 491–502 (2008). [PubMed: 19026780]
46. Ellwood-Yen K et al. Myc-driven murine prostate cancer shares molecular features with human prostate tumors. Cancer Cell 4, 223–238 (2003). [PubMed: 14522256]
47. Drost J et al. Organoid culture systems for prostate epithelial and cancer tissue. Nat. Protoc 11, 347–358 (2016). [PubMed: 26797458]
48. Ku SY et al. Rb1 and Trp53 cooperate to suppress prostate cancer lineage plasticity, metastasis, and antiandrogen resistance. Science 355, 78–83 (2017). [PubMed: 28059767]
49. Ran FA et al. Genome engineering using the CRISPR-Cas9 system. Nat. Protoc 8, 2281–2308 (2013). [PubMed: 24157548]
50. Pantelidou C et al. PARP inhibitor efficacy depends on $CD8^+$ T-cell recruitment via intratumoral STING pathway activation in *BRCA*-deficient models of triple-negative breast cancer. Cancer Discov. 9, 722–737 (2019). [PubMed: 31015319]
51. Schindelin J et al. Fiji: an open-source platform for biological-image analysis. Nat. Methods 9, 676–682 (2012). [PubMed: 22743772]
52. Lamprecht MR, Sabatini DM & Carpenter AE CellProfiler: free, versatile software for automated biological image analysis. Biotechniques 42, 71–75 (2007). [PubMed: 17269487]
53. Calagua C et al. Expression of PD-L1 in hormone-naive and treated prostate cancer patients receiving neoadjuvant abiraterone acetate plus prednisone and leuprolide. Clin. Cancer Res 23, 6812–6822 (2017). [PubMed: 28893901]
54. Bustin SA et al. The MIQE guidelines: minimum information for publication of quantitative real-time PCR experiments. Clin. Chem 55, 611–622 (2009). [PubMed: 19246619]
55. Dobin A et al. STAR: ultrafast universal RNA-seq aligner. Bioinformatics 29, 15–21 (2013). [PubMed: 23104886]
56. Trapnell C et al. Transcript assembly and quantification by RNA-seq reveals unannotated transcripts and isoform switching during cell differentiation. Nat. Biotechnol 28, 511–515 (2010). [PubMed: 20436464]
57. Buenrostro JD, Giresi PG, Zaba LC, Chang HY & Greenleaf WJ Transposition of native chromatin for fast and sensitive epigenomic profiling of open chromatin, DNA-binding proteins and nucleosome position. Nat. Methods 10, 1213–1218 (2013). [PubMed: 24097267]
58. Corces MR et al. An improved ATAC-seq protocol reduces background and enables interrogation of frozen tissues. Nat. Methods 14, 959–962 (2017). [PubMed: 28846090]
59. Langmead B, Trapnell C, Pop M & Salzberg SL Ultrafast and memory-efficient alignment of short DNA sequences to the human genome. Genome Biol. 10, R25 (2009). [PubMed: 19261174]
60. Zhang Y et al. Model-based analysis of ChIP-Seq (MACS). Genome Biol. 9, R137 (2008). [PubMed: 18798982]

Author Manuscript Author Manuscript Author Manuscript Author Manuscript

61. Bourgey M et al. GenPipes: an open-source framework for distributed and scalable genomic analyses. Gigascience 8, 10.1093/gigascience/giz037 (2019).

62. Zhu LJ et al. ChIPpeakAnno: a Bioconductor package to annotate ChIP-seq and ChIP-chip data. BMC Bioinformatics 11, 237 (2010). [PubMed: 20459804]

63. Yu G, Wang LG & He QY ChIPseeker: an R/Bioconductor package for ChIP peak annotation, comparison and visualization. Bioinformatics 31, 2382–2383 (2015). [PubMed: 25765347]

64. Lefebvre C et al. A human B-cell interactome identifies MYB and FOXM1 as master regulators of proliferation in germinal centers. Mol. Syst. Biol 6, 377 (2010). [PubMed: 20531406]

65. Szklarczyk D et al. STRING v11: protein–protein association networks with increased coverage, supporting functional discovery in genome-wide experimental datasets. Nucleic Acids Res. 47, D607–D613 (2019). [PubMed: 30476243]

66. Beltran H et al. Molecular characterization of neuroendocrine prostate cancer and identification of new drug targets. Cancer Discov. 1, 487–495 (2011). [PubMed: 22389870]

67. Abida W et al. Genomic correlates of clinical outcome in advanced prostate cancer. Proc. Natl Acad. Sci. USA 116, 11428–11436 (2019). [PubMed: 31061129]

Author Manuscript Author Manuscript Author Manuscript Author Manuscript

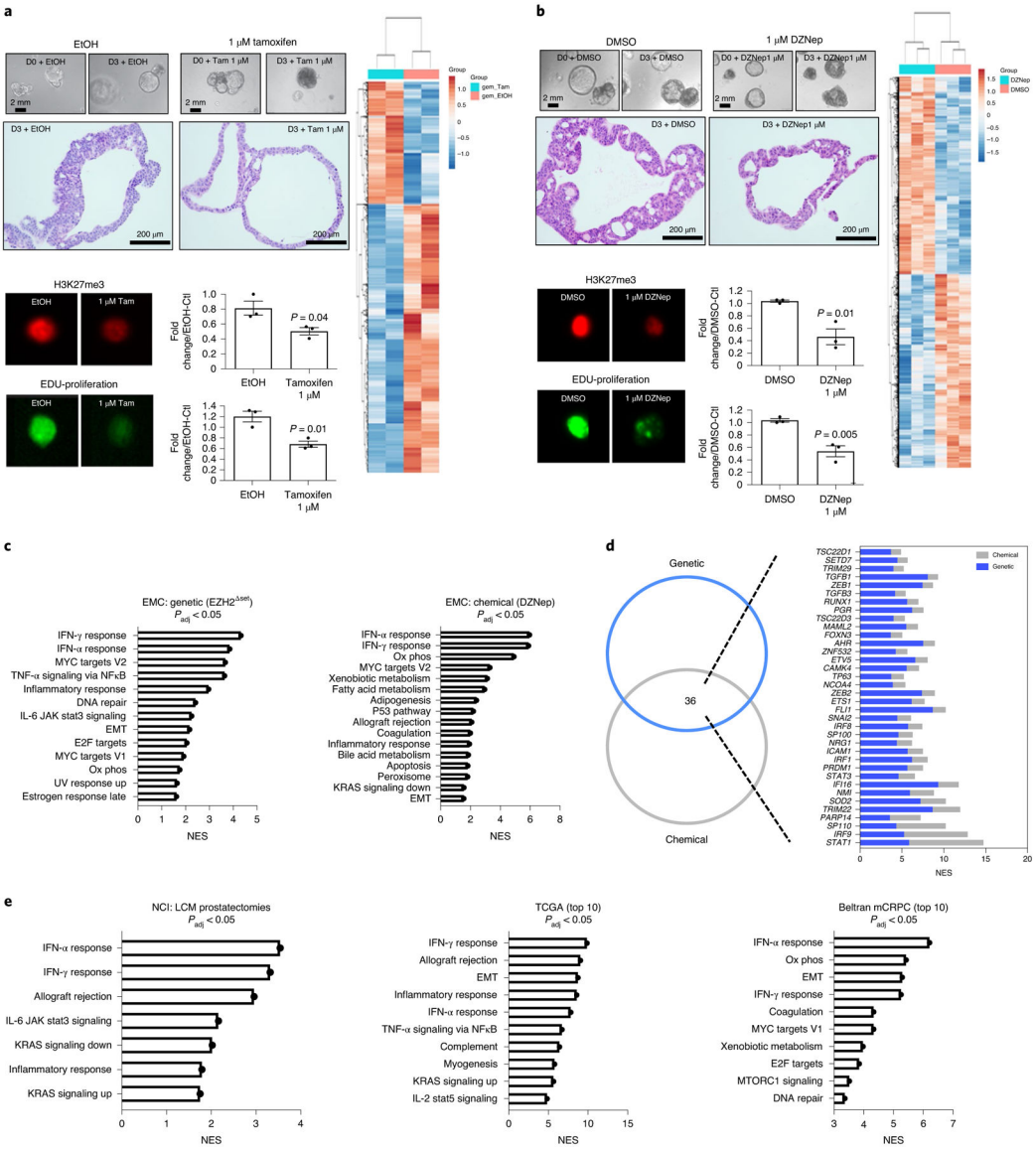

Fig. 1 |. EZH2 negatively regulates type I/II ISGs in PCa.

a,**b**, EZH2 catalytic activity in EMC PCa mouse organoids inhibited by genetic or chemical inhibition of EZH2 catalytic activity. Chemical and genetic EZH2 inhibition decreases H3K27me3, DNA replication and gene expression. Gene expression differentials were generated by RNA-seq. H3K27me3 and EDU (2′deoxy-5-ethynyluridine) signal intensity were analyzed by ImageStream flow cytometry. *P* values were generated using a two-tailed, unpaired Student's *t*-test with Welch's correction. Data were generated from $n = 3$ independent experiments and displayed as mean ± s.e.m. **c**, GSEA revealing enrichment of type I/II IFN gene signatures in mouse PCa organoids after EZH2 inhibition. Ox phos, oxidative phosphorylation. **d**, Master regulation analysis of RNA-seq data from 1C (overlap of top 200 TFs ranked by NES) enriched for TFs that regulate type I/II IFN-response genes. **e**, GSEA reveals enrichment of type I/II IFN gene signatures in human PCa patients with the lowest EZH2 activity. Sample numbers used are for NCI-laser capture dissection

prostatectomies (n = 21 samples), for the Cancer Genome Atlas (TCGA; n = 204 samples) and for Beltran mCRPC (n = 17 samples).

Author Manuscript Author Manuscript Author Manuscript Author Manuscript

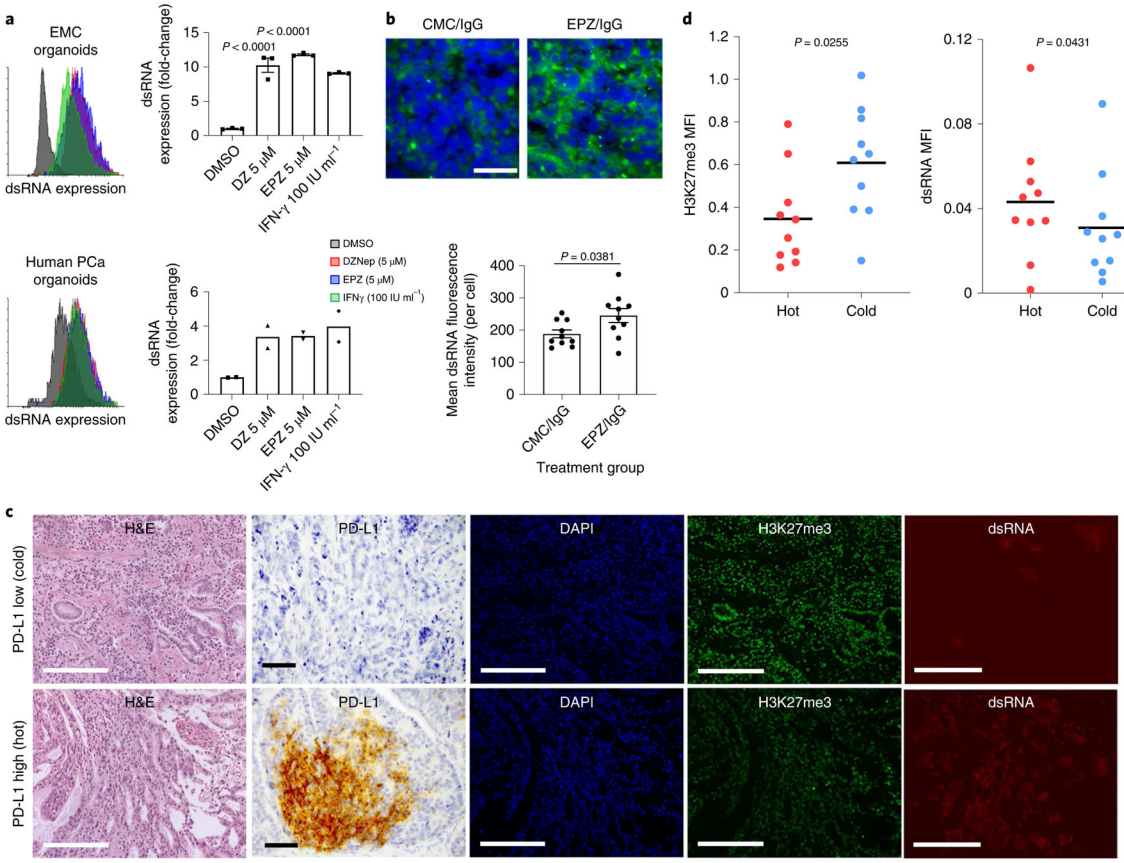

Fig. 2 |. EZH2 inhibition derepresses endogenous dsRNA.

a,**b**, Inhibition of EZH2 induces expression of dsRNA in mouse and human PCa organoids (**a**) and PCa tissue in vivo (**b**). Data for **a** were generated from $n = 3$ (EMC mouse) or $n = 2$ (human) independent experiments and $n = 10$ independent mice for **b**. Scale bars, 25 μm. *P* values for **a** were generated using a one-way ANOVA, Tukey's multiple-comparison test for **a** and a two-tailed, unpaired Student's *t*-test with Welch's correction for **b**, and displayed as mean ± s.e.m. **c**,**d**, Histopathology analysis of human prostatectomy samples indicating tumors with >5% PD-L1 tumor-positive staining (PD-L1 high, $n = 10$ patients) exhibits low H3K27me3 and high dsRNA staining. Tumors with <5% tumor-positive staining (PD-L1 low, $n = 10$ patients) exhibit high H3K27me3 and low dsRNA staining (**c**). **d**, Quantification of MFI for H3K27me3 and dsRNA staining performed in **c**. MFI, mean fluorescence intensity. Scale bars, 100 μm.

Author Manuscript Author Manuscript Author Manuscript Author Manuscript

Author Manuscript Author Manuscript Author Manuscript Author Manuscript

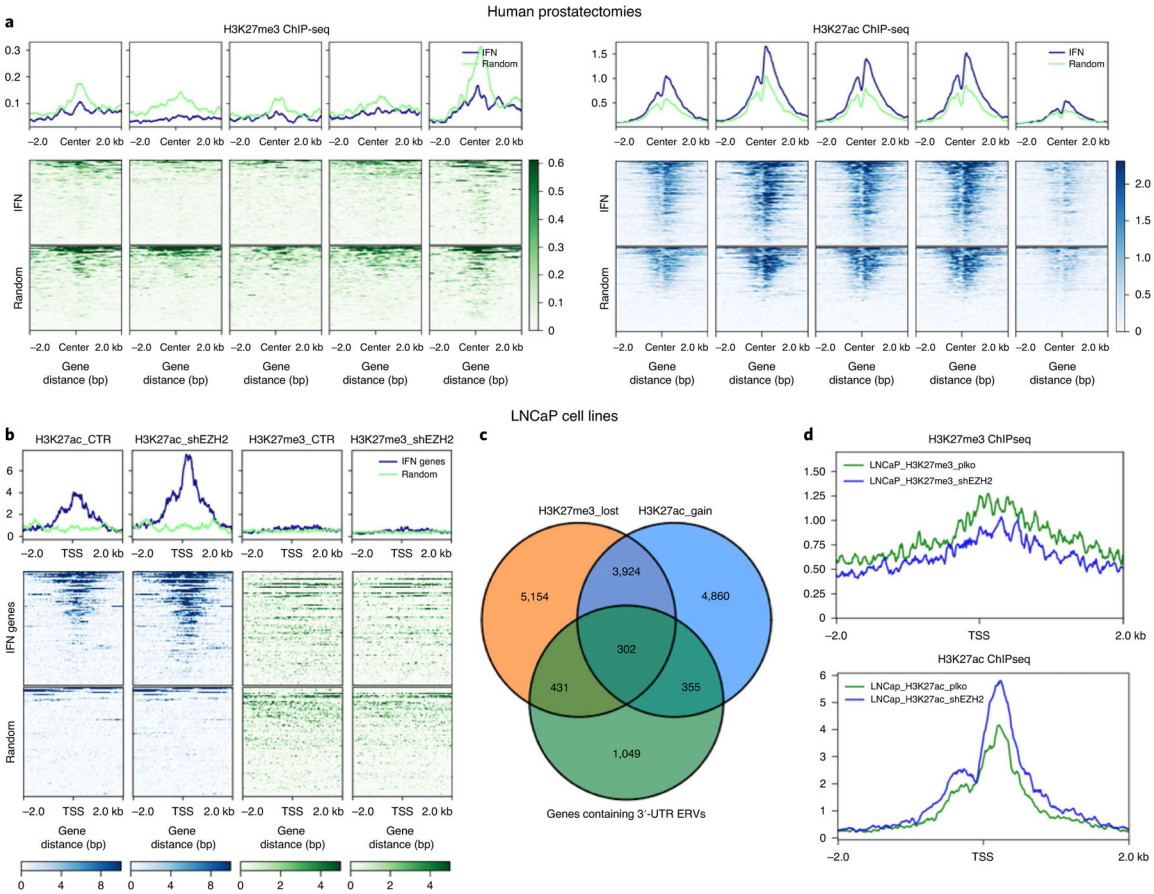

Fig. 3 |. ISGs are poised for activation by EZH2 inhibition.

a, Heatmaps of normalized H3K27me3 and H3K27ac signaling intensities of 97 ISGs from 5 independent patient prostatectomy samples. Each patient sample was analyzed once for each histone mark. The blue line represents the intensity signal of the 97 ISGs described in Extended Data Fig. 3 and the green line represents the signal intensity of randomly selected genes. **b**, LNCaP cell lines treated with nonspecific or EZH2-targeted short hairpins indicating, on EZH2 knockdown ISG display, no direct association with H3K27me3, but accumulation of increased H3K27ac. **c**,**d**, Venn analysis of LNCaP cell lines indicating a total of 302 genes that concurrently lose H3K27me3 and gain H3K27ac that also contain ERV sequences within their 3′-UTR that are upregulated after EZH2 knockdown. **d**, Average H3K27me3 and H3K27ac peak intensity associated with the the promoter regions of the 302 genes identified in **c**. Data for **b**–**d** were generated from previously published ChIP–seq data (accession no. GSE107780). There was a single replicate for each histone ChIP and the treatment condition was provided and used to generate data.

Author Manuscript Author Manuscript Author Manuscript Author Manuscript

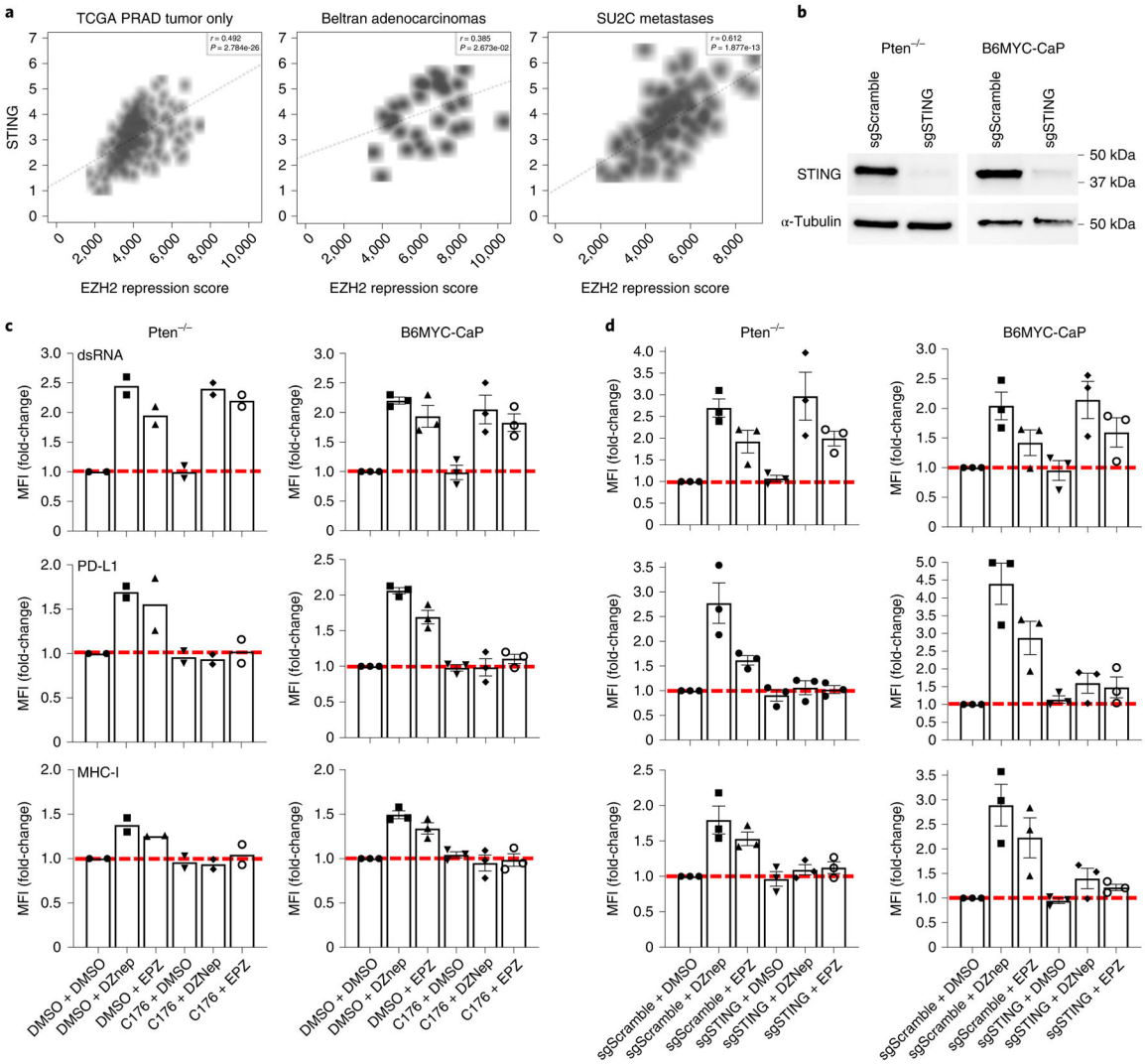

Fig. 4 |. Activation of ISGs is STING dependent.

a, Human PCa gene expression data demonstrating increased expression of the dsRNA sensor STING significantly correlated with low EZH2 catalytic activity. Sample numbers used are $n = 118$ samples for SU2C, $n = 408$ samples for TCGA and $n = 33$ samples for Beltran adenocarcinomas. **b**, Cropped western blots showing validation of STING KO in Pten$^{-/-}$ and B6-Hi*MYC*–CaP mouse PCa cell lines. Western blot analysis was performed once ($n = 1$ genotype/treatment condition). **c**,**d**, Chemical (**c**) or genetic (**d**) inhibition of STING demonstrating that EZH2 inhibitor activation of IFN-stimulated molecules, PD-L1 and MHC-I proteins, are dependent on STING activity. Data were generated using flow cytometry analysis from $n = 3$ independent experiments and displayed as mean ± s.e.m. *P* values can be seen in Extended Data Fig. 4 and were generated using a two-tailed, unpaired Student's *t*-test with Welch's correction. MFI, mean fluorescence intensity. Note that data from Pten KO cells in **c**, treated with C176 to inhibit STING, were generated from $n = 2$ independent experiments and displayed as the mean value. All values are presented as fold-change normalized to control conditions (DMSO + DMSO or sgScramble + DMSO). The red line indicates the normalized value of the control.

Author Manuscript Author Manuscript Author Manuscript Author Manuscript

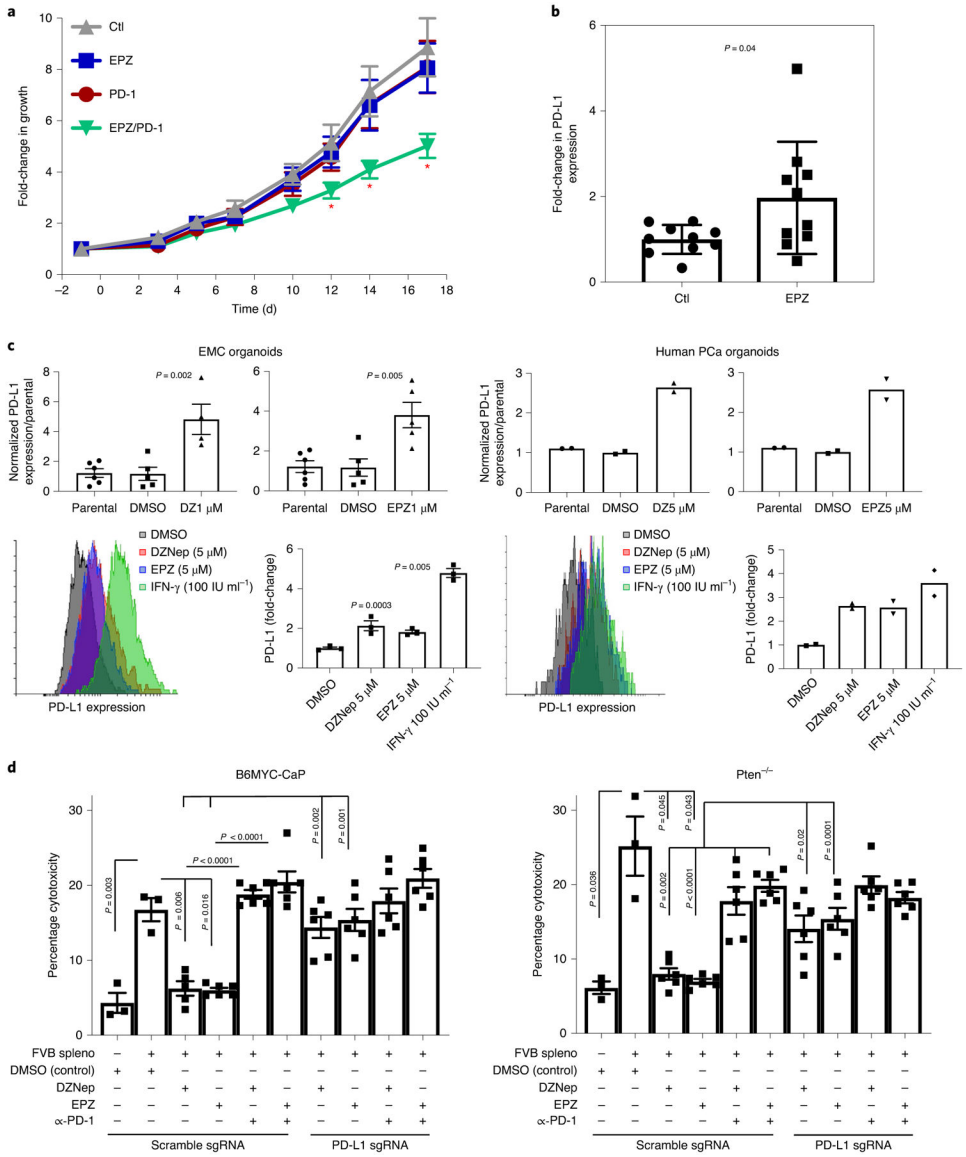

Fig. 5 |. EZH2 inhibition sensitizes murine prostate tumors to PD-1 CPI and is dependent on tumor PD-L1 activation.

a, EZH2 inhibition combines with PD-1 blockade to significantly inhibit prostate tumor progression in vivo. Each group consists of $n = 10$ mice. The P values were generated using a multiple Student's t-test. Asterisks represent: day 12, $P = 0.043$; day 14, $P = 0.017$; day 18, $P = 0.011$. **b**, EZH2 inhibition increases PD-L1 tumor expression ($n = 10$ mice/tumors per treatment group). The P values were generated using a two-tailed, unpaired Student's t-test with Welch's correction and displayed as mean ± s.e.m. Ctl, control. **c**, Mouse and human PCa organoids treated for 96 h with EZH2 inhibitors notably upregulating PD-L1 gene and protein expression. Data were generated from $n = 3$ (EMC mouse, left) or $n = 2$ (human, right) independent experiments and displayed as mean or mean ± s.e.m. The P values were generated using a one-way ANOVA, Tukey's multiple-comparison test and represent DMSO versus treatment. **d**, Upregulation of tumor PD-L1 expression functionally assessed using an in vitro cytotoxicity assay. Inhibition of immune cell cytotoxicity after EZH2 inhibition was

Author Manuscript Author Manuscript Author Manuscript Author Manuscript

rescued by PD-1 blockade. This rescue is dependent on tumor PD-L1 upregulation. Data were generated from $n = 6$ independent experiments and displayed as mean ± s.e.m. The P values were generated using a two-tailed, unpaired Student's t-test with Welch's correction. B6MYC-CaP and Pten$^{-/-}$ denote the murine 2D cell lines generated from the genetically engineered mouse models of PCa.

Author Manuscript Author Manuscript Author Manuscript Author Manuscript

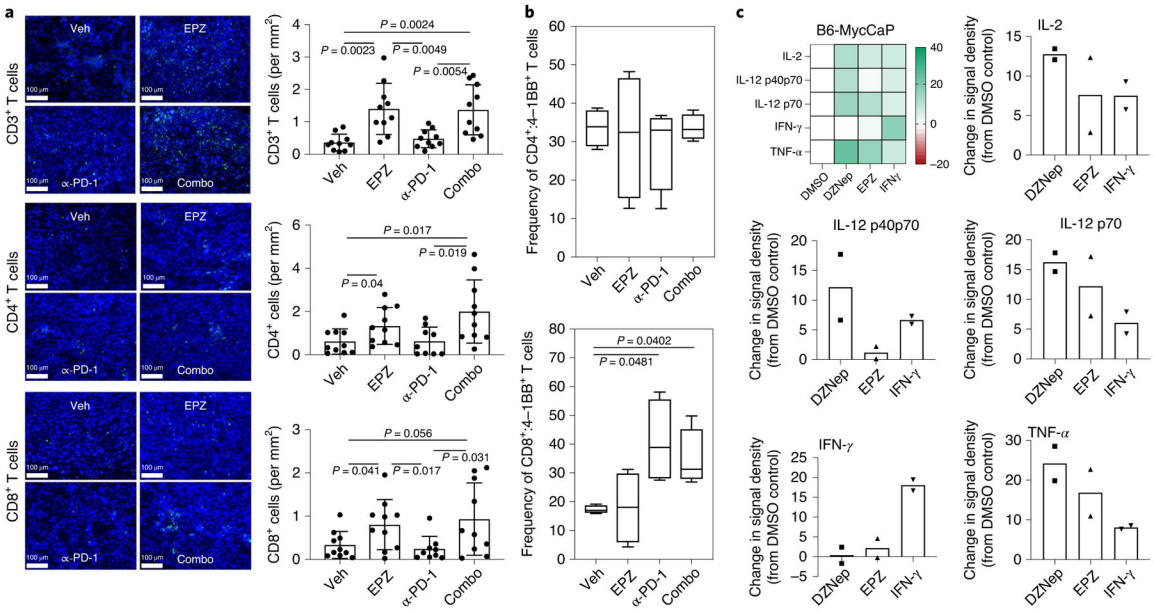

Fig. 6 |. EZH2 inhibition increases T-cell infiltration and induces PCa cell Th1 chemokine expression.

a, EZH2 inhibition alone or in combination (Combo) with PD-1 blockade significantly increasing $CD3^+$, $CD4^+$, $CD8^+$ tumor T-cell trafficking. Scale bar, 100 μm. Each group analyzed consisted of $n = 10$ mice. Data were generated by quantification of fluorescently positive cells using an EVOS FL Auto 2 Cell Imaging System. Immunofluorescent images represent scanned tumor samples. Veh, vehicle. **b**, PD-1 blockade alone or in combination significantly increased activated $CD8^+$ T cells but not $CD4^+$ T cells. Each group analyzed consisted of $n = 4$ mice. Box plots are displayed as minimum to maximum distribution. All *P* values for **a** and **b** were generated using a two-tailed, unpaired Student's *t*-test with Welch's correction. **c**, Murine B6-MycCaP PCa cells treated with EZH2 inhibitors increasing expression of Th1 chemokines. Data were generated by use of a cytokine western blot array and are displayed as the mean from $n = 2$ independent experiments.

Author Manuscript Author Manuscript Author Manuscript Author Manuscript

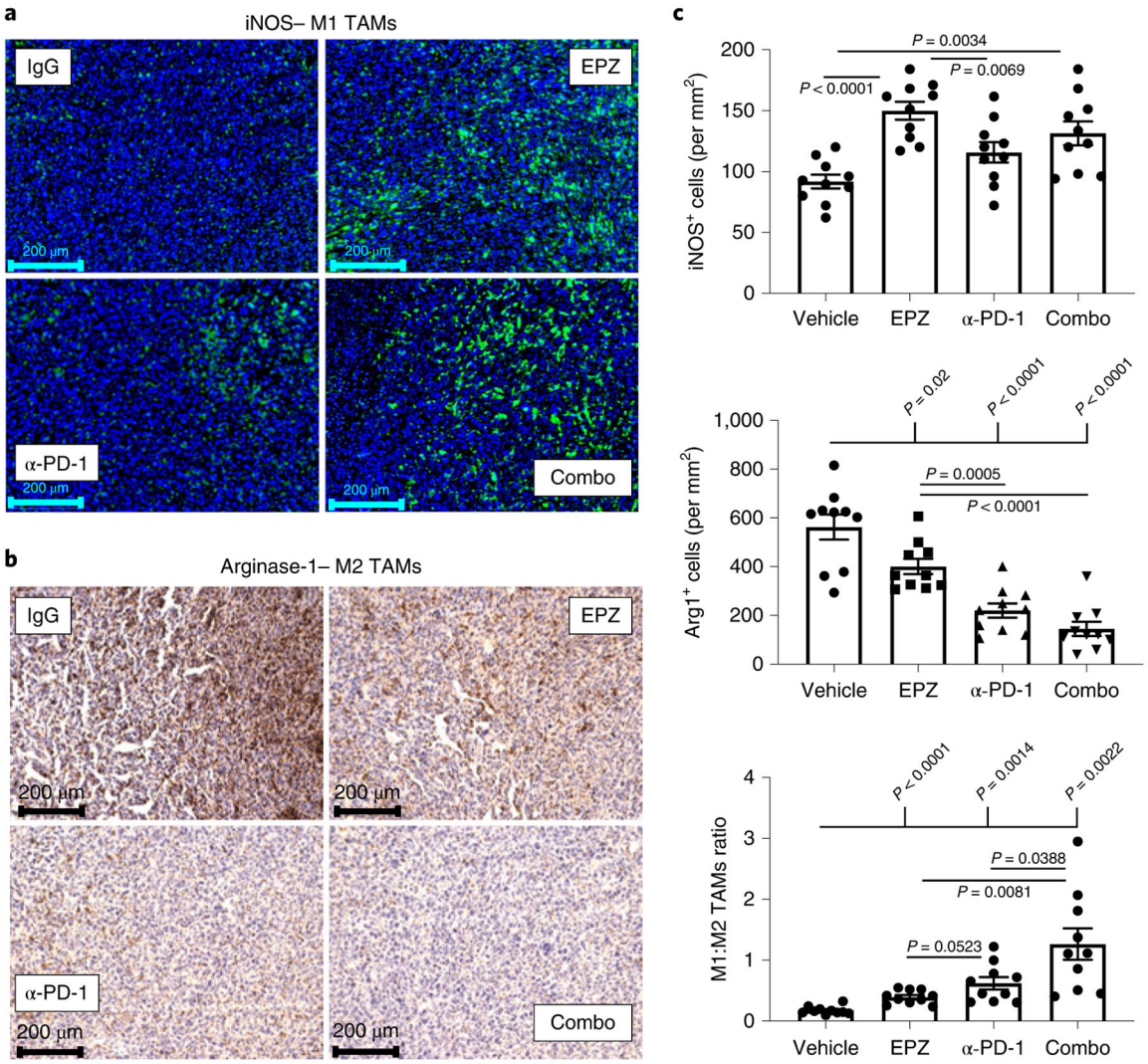

Fig. 7 |. EZH2 inhibitor combination with PD-1 CPI alters the immunosuppressive tumor microenvironment.

a,**b**, Example micrographs indicating alterations of M1 TAMs (**a**) and M2 TAMs (**b**) within the tumor microenvironment after treatment. Scale bar, 100 µm. **c**, Quantification indicating that combination therapy (Combo) provides the most significant overall changes to the tumor microenvironment M1:M2 TAM ratio. The *P* values were generated using a two-tailed, unpaired Student's *t*-test with Welch's correction. Each group analyzed consisted of $n = 10$ mice. Data were generated by quantification of fluorescent or 3,3′-diaminobenzidine-positive cells using an EVOS FL Auto 2 Cell Imaging System. Images represent scanned tumor samples.